Journal of Energy Storage 52 (2022) 104720

Contents lists available at ScienceDirect

Journal of Energy Storage

journal homepage: www.elsevier.com/locate/est

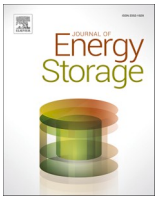

Review Article

A survey on lithium-ion battery internal and external degradation modeling and state of health estimation

G. Vennam [a], A. Sahoo [b,*], S. Ahmed [c]

[a] School of Electrical and Computer Engineering, Oklahoma State University, Stillwater, OK 74078, USA
[b] Division of Engineering Technology, Oklahoma State University, Stillwater, OK 74078, USA
[c] School of Civil and Environmental Engineering, Oklahoma State University, Stillwater, OK 74078, USA

ARTICLE INFO

Keywords:
Internal and external degradation models
Machine learning methods
State of health
Solid electrolyte interface
Incremental capacity analysis
Differential voltage analysis

ABSTRACT

Battery management system (BMS) is an integral part of the Lithium-ion battery (LIB) for safe operation and power management. The advanced BMSs also provide state of charge (SOC) and state of health (SOH) information. Accurate estimation of the SOC and SOH from a sparse set of input and output measurements (voltage, current, and surface temperature) is challenging due to the internal inter-related complex electrochemical side reactions. Several factors, such as charge/discharge rate, operating temperature, internal aging, abnormal charging-discharging cycles, and internal faults, adversely affect the LIB's health. To aid the development of intelligent and robust BMS with the capability of health-conscious decision making, a deep understanding of the internal degradation mechanisms and the effect of external degradation-inducing factors are of primary importance. This paper presents an in-depth review of internal and external degradation mechanisms at both anode and cathode of LIB with their corresponding mathematical models and correlation with SOH metrics (capacity and power fade). Different electrochemical models integrated with the internal degradation mechanisms and their governing equations are discussed and summarized. The effects of the external aging factors on capacity and power fade and the dominant degradation mechanism under cycling and stored conditions are also reviewed and tabulated for quick reference. Recent developments in BMS's capabilities for SOH estimation using advanced and intelligent algorithms under various internal degradation conditions are also presented. Finally, the challenges in modeling, estimation of SOH, and several future research directions for developing self-learning and smart BMS are provided.

1. Introduction

High energy density, low self-discharge rate, and longer life [1] of Lithium-ion batteries (LIBs) made it the common choice for powering both high and low power equipment. For instance, the recent plug-in electric vehicles (EVs) [2], with the LIB as the primary power source, successfully bridge the gap between the average range of EVs and their gas-powered counterparts. The new EV variants can also provide a range of 300 miles per charge. On the other hand, the EV community is also working relentlessly to reduce EV's charging time to a level close to gas-powered vehicle's fueling time. With the introduction of high power superchargers (450 kW) [3], the current charging time is reduced to 15 min to reach 80% of the state of the charge (SOC) level. These advancements in LIB and EVs are alleviating the user's *range anxiety* and paving the way for their ubiquitous acceptance.

However, it is well known that the volatility of internal constituents, flammability, reactivity, and toxicity of the electrolyte, which is the flip side of the high energy density LIBs, makes them thermally unstable at high temperatures and reduces life when operating at low temperatures [4]. The low tolerance to abuse (over-charging/discharging) and vulnerability to thermal runway jeopardize user safety, which is a primary concern. A battery management system (BMS) is employed for the safe operation, power and energy management of a LIB. The state-of-the-art BMSs are augmented with advanced SOC and state of health (SOH) estimation tools along with other traditional functions, such as voltage, current, and temperature monitoring, and cell balancing. A standard architecture of BMS with various SOC and SOH estimation functionality is shown in Fig. 1.

SOC is the ratio of the remaining capacity to the fully charged capacity of the battery. The SOC estimation dates back to the early 1980s,

* Corresponding author.
E-mail address: avimanyu.sahoo@okstate.edu (A. Sahoo).

https://doi.org/10.1016/j.est.2022.104720
Received 19 November 2021; Received in revised form 18 March 2022; Accepted 19 April 2022
Available online 12 May 2022

and ample reviews on SOC estimation schemes are available in the literature [5,6]. On the other hand, SOH is a figure of merit of a battery cell/pack's present condition compared to its ideal conditions. SOH linearly refers to capacity loss and power loss (the internal resistance increment), which quantifies the aging phenomena of LIB. SOH estimation is challenging and might not always be accurate due to the dependency on the time-varying internal degradation mechanisms. These inter-related degradation mechanisms include solid electrolyte interface (SEI) layer formations [7], metal dissolution, loss of contact between the active materials and current collector or carbon network (both cathode and anode), lithium (Li) metal plating, dendrite formations, and mechanical degradation of the electrodes (particle cracking). Although, there are several results available on modeling and analysis of internal degradation mechanisms and their interplay, they are not yet fully understood and are an active research area.

Primarily there are three SOH estimation methods, i.e., 1) experimental; 2) model-based; and 3) data-driven, proposed in the literature [8–10]. Surveys on empirical, model-based (recursive least square (RLS), Kalman filter (KF)), direct measurement (static measurement, electrochemical impedance spectroscopy (EIS)), and filter-based methods (Extended KF (EKF), particle filter (PF)) are available in the literature for a long time [8,11]. Likewise, intelligent SOH estimation methods using neural networks (NN), support vector machine (SVM), genetic algorithm (GA) along with model-based methods (RLS, EKF) are reviewed in [12,13]. For real-time applications, online SOH estimation methods utilizing NN, fuzzy logic (FL), deep NN (DNN) [14] in combination with degradation mechanisms were discussed in [15]. Similar reviews addressing different SOH estimation methods focusing on battery chemistry, data processing mode, processing time, algorithm, characteristics, accuracy, strength, and weakness are also presented in [16,17]. Recently, data-driven SOH estimation techniques using “big data” analytics, which have gained attention for its application in EVs with high accuracy, are reviewed in [10,18].

The focus of all the above review papers [8–11,16,17] is on SOH estimation process only without incorporating discussions on the internal degradation mechanisms. Since the SOH metrics (capacity and power fade) are orchestrated by both the internal and external degradation inducing factors and the mechanisms, a review that can explicitly discuss the correlations will be of paramount importance to the LIB research community. Although a few of the recent reviews [10,11] provided insights into internal aging mechanisms, such as loss of active material (LAM), SEI layer formation, and loss of Li inventory (LLI), these reviews did not discuss the modeling approaches for internal degradation mechanisms at anode and cathode, which can be integrated with traditional model based schemes to quantify SOH more accurately. Furthermore, reviews on recently developed advanced SOH estimation methods tethered with internal and external degradation are not available.

Motivated by the lack of a comprehensive review on LIB's degradation and its correlation with the SOH metrics and estimation, we present an in-depth review of the internal degradation mechanisms along with their mathematical models. We also review the advanced/emerging SOH estimation methods considering both the internal and external aging effects to identify the trend and research gap which hinders the development of intelligent BMS with health-conscious decision making capability. To the authors' best knowledge, this is the first time such a review encompassing internal degradation and health estimation is presented.

Contributions of the paper. The key contributions of this paper are the review of 1) modeling studies on internal degradation mechanisms at both anode and cathode, and their relation to SOH metrics, 2) different electrochemical models integrated with the internal degradation mechanisms, along with their governing equations, for commercially available graphite and metal anodes, 3) the individual and combined contributions of external aging factors to capacity and power fade along with the dominant degradation mechanism under cycling and stored conditions, 4) advanced SOH estimation methods accounting for the influence of both internal and external aging factors, and 5) empirical models of capacity and power fade for calendar and cycle aging with different cathode chemistry. Finally, we provide recommendations and

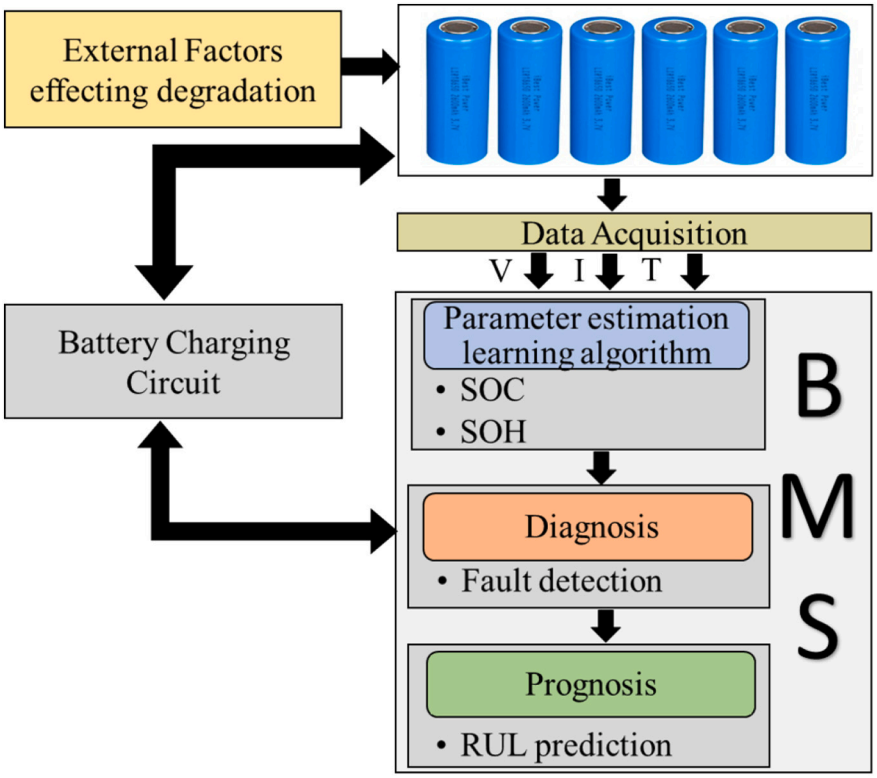

Fig. 1. The architecture BMS with SOC and SOH estimation, fault diagnosis and prognosis.

future directions for intelligent BMS development with self-learning capabilities.

The paper is organized as follows. The internal degradation mechanisms and their modeling are discussed in Section 2. The external factors affecting the degradation of LIB are discussed in Section 3. Section 4 deals with advanced SOH estimation methods. Finally, the review concludes in Section 6 with some recommendations and future direction in Section 5. The list of all abbreviations and nomenclature used throughout the paper are presented in Tables 1 and 2, respectively.

Table 1
List of all abbreviations.

ANN	Artificial neural network	KF	Kalman filter
BMS	Battery management system	LIB	Lithium ion battery
CEI	Cathode electrolyte interface	LLI	Loss of lithium inventory
CFD	Capacity fade deviation percentage	ML	Machine learning
DNN	Deep neural network	OCV	Open circuit voltage
DOD	Depth of discharge	PF	Particle filter
DVA	Differential voltage analysis	PDF	Probability density function
ECM	Equivalent circuit model	P2D	Pseudo 2D
EIS	Electrochemical impedance spectroscopy	RLS	Recursive least square
EKF	Extended Kalman filter	RUL	Remaining useful life time
EVs	Electric vehicles	SEI	Solid electrolyte interface
FL	Fuzzy logic	SOC	State of charge
GPR	Gaussian process regression	SOH	State of health
GRA	Grey relational analysis	SP	Single particle
HI	Health indicator	SVM	Support vector machine
ICA	Incremental capacity analysis	UPF	Unscented particle filter
ICL	Irreversible capacity loss		

Table 2
List of all nomenclature.

A	Cross sectional area (m^2)	R_g	Universal gas constant ($J\ K^{-1}\ mol^{-1}$)
Ah	Ampere-hour throughput	R_j	Radius of the particle (m)
$c_{\bar{k}}$	Concentration of species $\bar{k}$ ($mol\ m^{-3}$)	R_l	Rate of homogeneous reaction ($mol\ cm^{-2}\ s^{-1}$)
C_{loss}	Capacity loss	$R_{0_{inc}}$	Increase in internal resistance of the battery
c_0	Li^+ bulk concentration ($mol\ m^{-3}$)	$s_{\bar{k}l}$	Stoichiometric coefficient for species in reaction l
C_{rate}	Charge/discharge rate of the battery	T	Temperature (K)
C_{rated}	Nominal/rated capacity of the battery (A h)	T_a	Ambient temperature (K)
$\bar{c}_{1j}$	Surface concentration of the sphere ($mol\ m^{-3}$)	T_c	Core temperature (K)
c_+	Normalized concentration of Li-ions ($mol\ m^{-3}$)	t_+	Transference number
D_{eff}	Effective diffusivity ($m^2\ s^{-1}$)	V	Molar volume of Li ($m^3\ mol^{-1}$)
$D_{\bar{k}}$	Solvent diffusivity in SEI phase ($m^2\ s^{-1}$)	V_{oc}	Open circuit voltage potential (V)
D_s^0	Arrhenius diffusion constant	V_t	Terminal voltage of the battery (V)
E_a	Activation energy ($J\ mol^{-1}$)	y_{tip}	Dendrite tip position (m)
F	Faraday's constant ($C\ mol^{-1}$)	z	Coordinate direction normal to the anode (m)
I	Charge or discharge current (A)	α_c	Cathodic transfer coefficient
i_{Lf}	Flat limiting current density ($A\ m^{-2}$)	ρ_e	SEI's electronic resistivity (m)
i_n	Current density normal to dendrite tip ($A\ m^{-2}$)	ΔSOC	SOC variation
L	Thickness/growth of SEI layer (m)	ξ	Electric permittivity of the film ($C\ V^{-1}\ m^{-1}$)
n	Number of moles of electrons	Φ, ϵ	Phase filed variables, values ranging $0-1$
$N_{\bar{k}}$	Molar flux of the species ($mol\ cm^{-2}\ s^{-1}$)		

2. Internal degradation mechanisms and their modeling

The lithium-ion battery is composed of four components, namely cathode, anode, electrolyte, and separator, and its performance is dependent on various properties of its components. The characteristics of different LIB materials along with its applications are given in Table 3. The health degradation is caused by different mechanical, thermal, and chemical processes occurring inside the battery. Modeling and controlling these processes is complicated and involved, yet is very useful for accurate and efficient SOH estimation. The modeling of the internal degradation mechanisms includes modeling different internal chemical reactions contributing to change in SOH indicators. Fig. 2, adopted from [19], depicts various internal degradation mechanisms for LIB including anode, such as SEI-layer formation, electrode fracture, Li plating, dendrite formation, and cathode degradation. In this section, we have discussed various anode and cathode degradation mechanisms and their corresponding mathematical models.

2.1. Anode degradation

2.1.1. Solid electrolyte interface (SEI) layer formation

The SEI layer formation at the electrode-electrolyte interface was first introduced in 1979 [20]. The solvents (intercalated Li) and Li-salt (electrolyte) forms a passivating layer (products of decomposed electrolyte) at the active electrode surface and grows in width substantially with consecutive charge and discharge cycles. This layer allows Li-ion transportation across the electrode and electrolyte and restricts electron tunneling, preventing continuous electrolyte decomposition. The SEI layer also protects against anode corrosion and maintains the battery's chemical and electrochemical stability by prohibiting further electrolyte reduction during cycling. Despite the above advantages of the SEI layer, active Li and electrolyte materials are consumed during layer formation and the internal resistance also increases, which are the orchestrating factors for capacity fade and low power density, respectively.

The SEI layer is formed during the first charge-discharge cycles of the battery on the anode (carbon electrodes), as shown in Fig. 2. It is one of the main aging factors of a graphite electrode (the most common choice of the anode) [21]. The reduction reactions and considerable volume expansion of the anode materials cause the SEI to be more unstable than on the cathode [22]. Over the years, extensive studies on anode SEI films have been reported in the literature.

The SEI's complicated structure, due to the electrolyte reduction reactions near the electrode surface, and the structural–property relationships play an essential role in modeling the SEI layer. These factors make the modeling process complex, leading to trial-and-error-based approaches [23]. In [20], a first attempt is made to model the SEI. The electron leakage through the SEI layer is considered a constraint for SEI growth. A growth rate SEI layer model is given by [20],

$$\frac{dL}{dt_{storage}} = \frac{\overline{K} V_{oc}}{\rho_e L} \tag{1}$$

where L is the thickness/growth of the SEI layer, $t_{storage}$ is storage time, $\overline{K}$ is constant, V_{oc} is open circuit potential, and ρ_e is the SEI's electronic resistivity. Since SEI is formed during the first charge-discharge cycle of the battery, it is also necessary to consider model equations that describe Li's mass transport in solid phases. The diffusion of Li-ions in an active solid particle is, in general, expressed using Fick's law [24], given by

$$\frac{\partial c_{\bar{k}}}{\partial t} = D_{\bar{k}} \left(\frac{\partial^2 c_{\bar{k}}}{\partial z^2} + \frac{2}{z} \frac{\partial c_{\bar{k}}}{\partial z} \right) \tag{2}$$

where $c_{\bar{k}}$ is the concentration of species $\bar{k}$, $D_{\bar{k}}$ is the solvent diffusivity in the SEI phase, z is the coordinate direction normal to the anode, and t is the time variable. A one-dimensional solvent diffusion model through

Table 3
Lithium-ion battery's material characteristics and applications.

LIB's name	Electrodes	Key benefits	Limitations	Applications
Lithium Cobalt Oxide (LCO)	$LiCoO_2$/ graphite	High specific energy	Low inherent safety; due to the low thermal stability of cobalt-oxide, cycle life is relatively modest, and high cost.	Sony
Lithium iron phosphate (LFP)	$LiFePo_4$/ graphite	Durability, good thermal stability, inherent safety and reliance on abundant eco-friendly materials, low cost	Sensitive to temperature variation and low specific energy in the range of 90-140 Wh/kg	BYD
Lithium manganese spinel (LMO)	$LiMn_2O_4$/ graphite	Low internal resistance yields in a relatively high specific power, LMO batteries have a longer cycle life than LCO, typically in the range of 1000–1500 cycles, inherently safe	Lower energy density, in the range of 100–140 Wh/kg	Nissan
Lithium nickel cobalt aluminum oxide (NCA)	Li^1/graphite	Outstanding specific energy in the range of 200–250 Wh/kg as well as high specific power	Marginally safe, and high cost.	Tesla, Daimler
Lithium nickel, manganese cobalt oxide (NMC)	Li^2/graphite	High specific energy	Compared to NCA, the NMC battery has lower energy density typically in the range of 140–200 Wh/kg, and high cost	Toyota, Volkswagen, General Motors
Lithium titanate (LTO)	(LMO, NCA)/Li^3	Highly safe, long life cycle span	Low specific energy in the range of 30–110 Wh/kg	Honda, Samsung, Toshiba

Li^1-$Li(Ni_085CO_0,1Al_005)0_2$, Li^2-$Li(Ni_0,33Mn_0,33Co_033)O_2$, $Li^3 = Li_4Ti_5O_{12}$.

the SEI layer is adopted in [25]. Film growth rate, resistance, and the irreversible capacity loss (ICL) are estimated using a simplified dilute solution theory by considering the transport of both Li+ ions and electrons through the SEI. The material balance equation in [24] is modified in [25] to account for variable film thickness ($L(t)$), as follows,

$$\frac{\partial c_{\bar{k}}}{\partial t} - \frac{\partial L}{\partial t}\frac{\partial c_{\bar{k}}}{\partial \xi}\frac{\xi}{L(t)} + \frac{1}{L(t)}\frac{\partial N_{\bar{k}}}{\partial \xi} + \sum_l s_{\bar{k}l} R_l = 0 \tag{3}$$

where $\frac{\partial L}{\partial t}$ is the film growth rate, $N_{\bar{k}}$ is the molar flux, R_l is the rate of homogeneous reaction in the film, $s_{\bar{k}l}$ is the stoichiometric coefficient for species in reaction l, and ξ is the electric permittivity of the film. If the film growth rate $\frac{\partial L}{\partial t}$ is slow, the second term in Eq. (3) can be neglected, and Eq. (2) is recovered to describe the transport of solution species limited to solid diffusion [24]. A similar one-dimensional model, which considers both solvent diffusion and kinetics of SEI formations [26], is developed in [27].

All the above models, focusing on the SEI layer formation process, lack in predicting the cycling behavior of LIB at different operating conditions along with the associated SEI growth processes. A multi-physical pseudo 2D (P2D) [26,28–31] SEI layer model, focusing on bridging the transport processes (charge balance, mass balance, energy balance) with elementary reaction-based SEI growth, is developed in [26]. Here, the diffusion rate-determining passive film thickness is given as,

$$L(t) = 2\lambda\sqrt{D_s^0 e^{\frac{-E_a}{R_g T}} t} \tag{4}$$

where D_s^0 is Arrhenius diffusion constant, E_a is the activation energy, R_g is the universal gas constant, T is the temperature, and $\lambda = \frac{c_+ e^{-\lambda^2}}{\sqrt{\pi} C_{Li_2Co_3} erf(\lambda)}$. Unlike the 1-D model, the concentration of Li [32] inside the solid phase is solved at each node point (j) along the radial coordinate, which is given by [32].

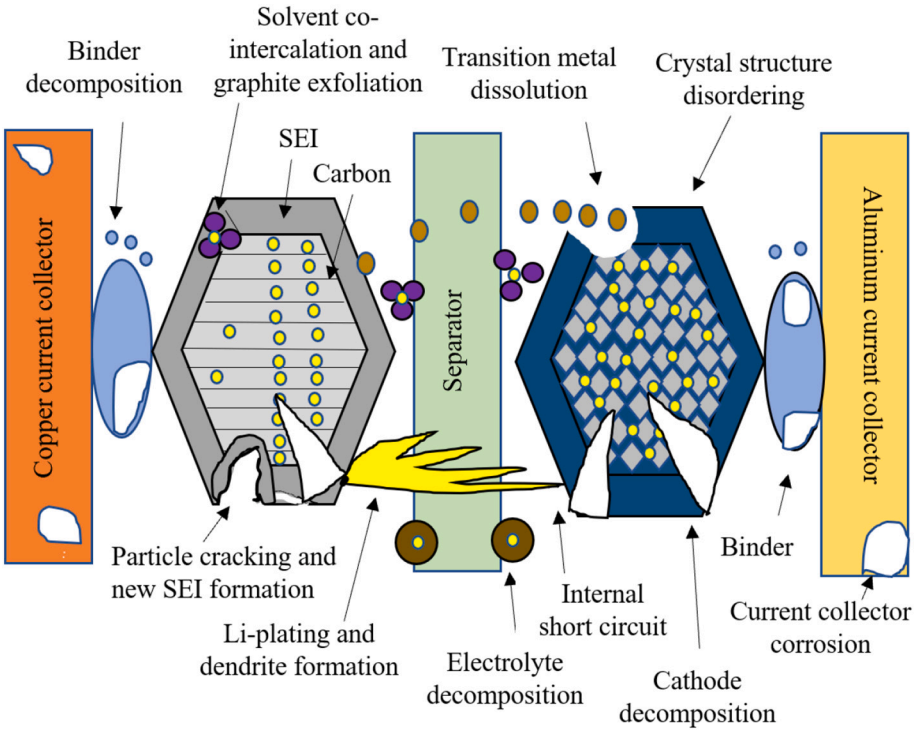

Fig. 2. Internal degradation mechanisms in Li-ion cells adopted from [19].

$$\frac{\partial c_{\bar{k},j}}{\partial t} = \frac{D_{\bar{k},j}}{z^2}\frac{\partial}{\partial_z}\left(z^2\frac{\partial c_{\bar{k},j}}{\partial z}\right). \quad (5)$$

A similar P2D model coupled with the 1D porous electrode model is developed in [28]. The proposed multiscale and multi-physics model reveals the effects of diffusivity, temperature, and kinetics on SEI growth.

The major limitation of the P2D model is the coupled nonlinear partial differential equations and high computational complexity. To overcome this limitation, a single particle (SP) model [33] was introduced. Electrodes are represented by a single spherical particle whose surface area is equivalent to the solid phase's active area in the porous electrode. This model considers a lumped parameter approach and reduces Eq. (5) to a first-order partial differential equation [33] given by

$$\frac{\partial c_{\bar{k},j}}{\partial t} + \frac{15D_{\bar{k},j}}{R_j^2}\left(c_{\bar{k},j} - \bar{c}_{1,j}\right) = 0, \quad (6)$$

where $\bar{c}_{1,j}$ is the surface concentration of the sphere, R_j is the average radius of the particles that constitute the electrode. Eq. (6) also eliminates the dependence on the spatial variable z. In [34], the SP electrochemical model coupled with thermal dynamics is developed to include temperature in SEI layer modeling. This coupled model can be used to provide insight into controlling the major technological hurdles of current interest, i.e., capacity loss under low temperature, much-reduced performance at subzero temperatures, and thermal runaway at high temperatures. Moreover, from the properties and functionalities, the SEI growth rate is also determined by modeling the electron tunneling and presented in [28]. Dual-layer SEI emerges from different electrolyte decomposition reactions. The studies on dual-layer SEI's are obtained by adding a second SEI formation reaction. The two layers of SEI differ in chemistry and morphology and grow simultaneously. Analysis of each SEI layer provides us information on fluctuations in SEI thickness and the relation to the rate-limiting transport mechanism in the solid SEI phase. Opposed to single-layer SEI's, dual-layer SEI formations consider two transport mechanisms, i.e., solvent diffusion and charge transport. Studies revealing the behavior of such dual layer structures are discussed in [35–37]. In [37], a double layer at the SEI-electrolyte and the particle-SEI interface are included in a model-based study of the aging-dependent processes. The physicochemical SP model in [34] has been extended by introducing a new aging model, which includes the SEI, to analyze the degradation of the LIB. The initial thickness of the SEI (L_0), is represented as [37],

$$L_0 = \frac{V_{SEI}R_a}{3\epsilon_{s,a}A_{cell}d_a} \quad (7)$$

where $\epsilon_{s,a}$ is the anode solid phase volume fraction, R_a is anode particle radius, d_a is the thickness of the anode, $V_{SEI} = \frac{n_{loss}M_{Li_2CO_3}}{2\rho_{Li_2CO_3}}$, with n_{loss} as the amount of lost Li, M_{Li2CO3} and ρ_{Li2CO3} as the molar mass and density of Li carbonate, respectively, and A_{cell} is the area of the cell.

The SEI layer modeling discussed above plays a prominent role in determining the SOH of LIBs. However, SEI is permeable to Li-ions. So, during the charging and discharging of the battery, large stresses are generated due to the volume expansions and contractions of the anode. Cycling also induces graphite exfoliation due to interaction between the solvent and graphite after diffusion through the SEI. These phenomena result in the electrode's fracture and further growth of fresh SEI, leading to capacity fade of the battery. The fracture mechanism and mechanical fatigue of the batteries are discussed next.

2.1.2. Fracture

The volume expansion and contraction of the electrodes during charging and discharging of the battery, respectively, build up internal stress leading to fractures/cracks on the electrodes. Upon cycling the battery, the fracture on the electrode surfaces grows gradually. The SEI layer grows on the newly exposed electrode surfaces consuming Li. It also increases the existing SEI thickness, resulting in additional Li loss and increase in resistance. Thus, this mechanical degradation caused by diffusion-induced stresses (DIS) is another significant contributors to capacity fading.

The DIS on electrodes have been studied and modeled in [38,39]. A stress generation model is developed in [38] to predict fractures in active electrode material of Li-ion cells based on two regimes (one phase and two phase material). Stresses calculated based on these regimes indicate that high-rate application require smaller particles (particle size) and avoid two phase regime to prevent over-discharge. Although DIS modeled in [38] are helpful in analyzing stresses and increase mechanical durability, the model lacks the inclusion of concentration dependence of Young's modulus, which significantly affects peak stress and stress evolution in the electrodes. The above limitation was later addressed in [39]. The models in [38,39] focused on understanding the host particle pulverization, i.e., DIS causing large Li concentration gradients at host electrode particles during high C_{rate}, where C_{rate} is the measurement of the charge and discharge current with respect to its nominal capacity. However, the study failed to explain higher coulombic loss during low C_{rate} than during storage, which can be attributed to the SEI layer's possible mechanical degradation.

Fractures of the SEI layer, which is caused due to exertion of large magnitude stresses during the expansion/contraction of an electrode particle, is studied in [40]. The authors concluded that the stresses experienced by the SEI leading to fracture and reforming at low C_{rate} as the dominant mechanism of cell capacity loss. The mathematical formulation relating SEI cracking to capacity fade during cycle aging is given as [40],

$$C_{cycloss} = a(\Delta SOL)^2 \quad (8)$$

where ΔSOL is the state of lithiation swing, $a>0$ is a constant and a function of diffusion properties of Li in the electrode material, rate of reaction, temperature, number of Li atoms involved in the reaction, radius of particles, and mechanical properties of SEI and electrode material. Recently [41], the evolution of DISs and concentration of Li-ions have been evaluated using an analytical model to determine the SEI's fracture mechanism and the fatigue in LIBs. In [42], the battery's capacity loss is examined as capacity fade deviation percentage (CFD) and it is also shown that, as the CFD increases, the crack propagation is dominant along with the influence of SEI layer growth on battery capacity loss.

Besides SEI layer formation and fracture, the other side reaction requiring attention to extend the existing coupled chemical/mechanical degradation models is Li plating. The determination of Li plating is crucial for efficient battery operation without compromising its life and safety. Li plating mechanism and modeling approaches to study capacity loss induced by itself are discussed next.

2.1.3. Lithium-ion plating

Li plating occurs after few charge and discharge cycles [4], where the SEI layer grows at the anode reducing the porosity of anodes. The porosity reduction leads to a local potential gradient rise at the anode-electrolyte interface, promoting Li metal formation at the narrow gap between the anode and the electrolyte. Li plating occurs when negative electrode surface potential falls below zero volts with respect to Li/Li^+ reference electrode.

The Li-ions are inclined to form metallic Li, particularly at low temperatures and during charging. Low temperatures (5°C) usually lead to decreased diffusion of Li within the SEI and graphite, which can overlay the electrode with Li plating [43,44]. In general, the deposited metallic Li is reversible. However, Li dendrites can lose contact with the active material during the oxidation process leading to dead Li in the cell. Furthermore, the plated metallic Li is also highly reactive and forms an irreversible SEI with the electrolyte. Conversely, Li stripping occurs if

the negative electrode potential reaches a positive value during the discharge process.

Li plating decreases the amount of cyclable Li-ions or increases the amount of frozen Li in the SEI layer between the electrodes that manifests itself as a reduction in capacity. The Li metal also increases Li plating's positive feedback, leading to an increase in battery resistance. Thus, the modeling of Li-ion plating is essential in analyzing aging and safety issues at lower temperatures.

Physicochemical models predict the onset of Li deposition and the possible amount of deposited metallic Li. An initial approach to describe the conditions for Li deposition during overcharge is presented in [45]. Here Doyle's model [29] is extended to include a side reaction described by the Butler-Volmer equation. Modifying this model, a reduced-order controls oriented cell degradation model is developed in [46]. Further, the model in [45] is also modified by the authors in [47] to include the effects of temperature (Arrhenius law—Section 3.1). A similar physics-based LIB aging model is presented in [4] by accounting for Li plating and SEI growth and predicting the transition from linear to nonlinear aging after extended cycling. The material balance equation employed for Li-metal is expressed as [4],

$$\frac{\partial C_{Li}}{\partial t} = -\frac{j_{lpl}}{F}(1-\beta) \tag{9}$$

where C_{Li} is the molar concentration of Li metal per unit volume of electrode, j_{lpl} is the transfer current density of Li deposition reaction, and parameter β is introduced, which denotes the fraction of plated Li that becomes SEI.

In addition, the degradation effects caused by Li-plating and Li-stripping simultaneously at low temperatures are also not discussed. Later, the authors in [48] developed a quantitative detection method for Li plating and included a study of electrochemical models incorporated with both Li plating and stripping reactions to investigate the process at low temperatures (− 5°C). Further, less complicated reduced-order models are developed in [49] to quantify the negative electrode potentials to predict Li plating's onset by considering the degradation effects, such as LLI, LAM, growth of plated Li, and secondary SEI and consumption of electrolyte solvents.

2.1.4. Dendrites

Li-dendrites are electrode surface protrusions that grow under activation and deposit on the electrode's flat surface during the diffusion process. These protrusions are often a result of Li-plating at the anode. Dendrites usually resemble a tree-like structure and grow only at above critical over potential values. The different growth sites for the dendrite include screw dislocations, nuclei of higher indices, or twinned structures [50]. Therefore, the formation of dendrites causes irreversible consumption of Li inventory and increases the charge transfer resistance due to the accumulation of dead Li [51]. Dendrites formation can also penetrate the separator and short-circuit the electrodes, which further aggravates Li metal's exothermic reactions with the electrolyte.

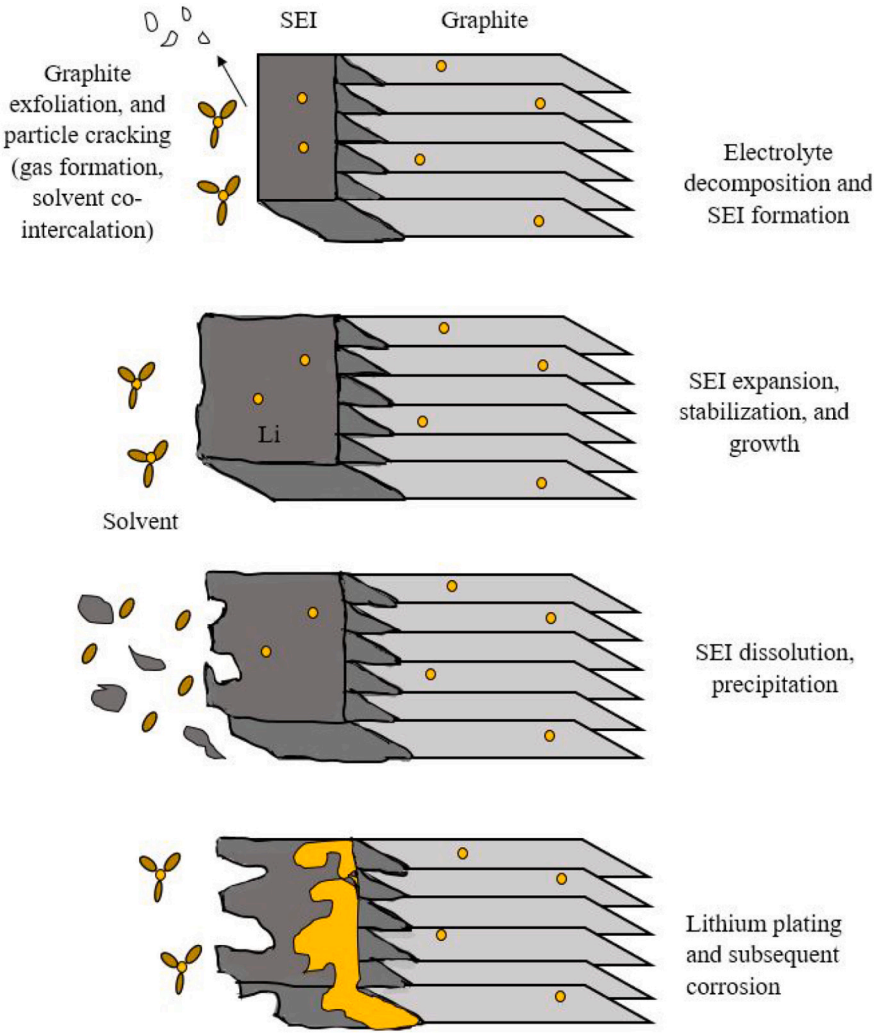

Fig. 3. The aging effects on anode (carbon/graphite) adopted from [7] with author's permission.

The formation and growth of Li dendrites can be categorized into two groups as 1) tip-growth mode [52], and 2) root-growth mode [53]. The modeling and analysis of tip-growth is extensively researched compared to root growth. It is based on Fick's law (Eq. (2)), incorporating various other effects, such as electric current, surface energy, and mechanical deformation. The first attempt was made in [54] to simulate the electrochemical dendrite growth and proposed a comprehensive mathematical model of the time evolution of dendrite tip height (Eq. (10)) and growth velocity in Li-polymer batteries, given by [54].

$$\frac{\partial y_{tip}}{\partial t} = \frac{V}{F} i_n \left(y_{tip}, t\right) \tag{10}$$

where y_{tip} is the dendrite tip position, V is the molar volume of Li, F is Faraday's constant, and i_n is current density normal to dendrite tip.

A simplified modeling approach analyzing the various over potentials underplay at the dendrite tip and the flat electrode surface is developed in [52]. The modeling work constitutes liquid electrolytes, and the analysis of various over potentials lead to a simplified dendrite tip current density expression in terms of various system parameters, such as operating current density, electrodeposition kinetics, and transport properties, when compared to the computationally complex expression in [54]. The current density expression is given as [52]

$$\frac{i_t}{i_f} = -\frac{1}{bc_0} ln\left[e^{-bc_0} + \frac{i_f}{i_{Lf}}\left(1 - e^{-bc_0}\right)\right]^{-\frac{\alpha_c}{n}} \tag{11}$$

where α_c is the cathodic transfer coefficient, ratio i_t/i_f represents the ratio of the dendrite tip current density to the current density on the flat surface, i_{Lf} is flat limiting current density, n is the number of moles of electrons, c_0 is the Li^+ bulk concentration and, the parameter b represents the concentration dependence of the diffusion coefficient. Later this model is extended to quantify the dendritic growth (i_t/i_f) during Li electrodeposition at a sub-ambient temperature [55].

All these models involve the solutions to the Nernst Planck equations [56] in the electrode or electrolyte, coupled with the electrochemical reactions at the electrode-electrolyte interfaces, given by

$$\frac{\partial c_+}{\partial t} = \frac{\partial}{\partial x}\left[D^{eff}\frac{\partial c_+}{\partial x} + \frac{(1 - t_+)I}{FA}\right] \tag{12}$$

where c_+ is the normalized concentration of Li-ions in an electrolyte, D_{eff} is effective diffusivity, t_+ is the transference number, A is the cross-sectional area, constant current I applied between $x = 0$ and $x = l_{cell}$ with l_{cell} is the length of a cell.

The electrode-electrolyte interface positions in the above models are assumed to be fixed, making them difficult to capture the complex moving interfaces and their morphological changes during the electrochemical processes, such as the Li dendrite growth in the cell. To overcome the above limitation, a phase-field method is proposed in [57] to simulate the continuous phase transition (evolution process) at the solid-liquid interface and Li dendrite's growth process. In this method, the Nernst Planck equation in Eq. (12) is modified to include the phase filed variables Φ and ϵ as follows [57],

$$\frac{\partial c_+}{\partial t} = \Delta\left[D^{eff}\Delta c_+ + \frac{D^{eff}c_+}{R_g T} nF\Delta\Phi\right] + r_t \tag{13}$$

where r_t is the source term containing phase field variable ϵ given as $r_t = -\overline{K}_1\frac{\partial\epsilon}{\partial t}$, $\overline{K}_1$ is the accumulation constant. All the modeling approaches proposed above provide deep insights into the physics of the formation and growth of Li dendrites on Li metal electrode. Studies related to the Li dendrite formation on graphite electrodes at room temperatures and low charge rates are given in [58–61]. Unlike graphite electrodes where Li plating may be reversible, Li metal anodes cause irreversible Li-dendrite

Table 4
A summary of internal degradation mechanisms and their modeling approaches.

Internal degradation	Modeling approaches	References	Remarks	Software
SEI	Parabolic models/one-dimensional model	[20,25,27,68]	The models account for variable film thickness and provide a broad, and fundamental understanding of the SEI; models focused on the SEI layer formation process while the battery level models are simplified.	CFD [68].
	A multi-physical pseudo 2D (P2D) model	[26,28,29,31]	Coupled SEI growth model with the accurate battery level model are provided for a more accurate prediction than 1D models; models have long simulation time due to the large number of nonlinear equations and coupled nonlinear partial differential equations.	COMSOL Multiphysics [26]
	Single particle (SP) model	[33,37,42]	The models improve computational run time without compromising accuracy; can be simulated quickly but suffers precision at high C_{rate} due to the lack of electrolyte physics and degradation is not taken into account.	MATLAB [37,69]
Fracture	Coupled chemical/mechanical degradation model	[70–73]	The models couples electrochemistry, chemical degradation (including SEI formation), and fracture mechanics so as to clarify life performance of a Li-ion cell, the models have high prediction accuracy with reduced computation complexity; fracture of the SEI can lead to the reduction of the electrolyte (that penetrates through the cracks) regenerating the SEI and henceforth increasing its thickness.	COMSOL Multiphysics [70]
Li plating	Physicochemical models	[4,45,47]	Li plating occurs at higher currents or lower ambient temperature; anode polarization and Li intercalation kinetics play a crucial role in determining the propensity of Li deposition; deposition of metallic Li on the surface of the anode particles together with the initiation of dendritic growth of Li is the most probable cause for a short circuit.	CFD [47]
	Reduced order models	[46,74]	The models are simple enough to be executed quickly on an inexpensive embedded systems processor.	COMSOL Multiphysics [46]
Dendrite growth	Tip growth-physical models	[52,54,75]	The dendrite growth is always slowed by lowering the current density; Li dendrites can detach from the electrode surface, leaving loose Li crystals called “dead” Li, which is a major source of battery energy density loss; unlike the SEI layer, Li dendrite formation is not acclaimed.	COMSOL Multiphysics [75]
	Phase field modeling	[57,76,77]	The models are used for modeling temporal and spatial microstructure evolution of materials undergoing a wide variety of processes, such as phase transformations, deformation, and particle coarsening.	COMSOL Multiphysics [77]
Cathode degradation	Chemical/mechanical degradation model	[64,65]	Cathode degradation is caused due to changes in the surface structure of particles and the electronic disconnection between the active materials and a current collector; models are useful for gaining insight into possible degradation mechanisms and could be more robust than pure empirical approaches; models are computationally complex, and have many parameters which may be unknown.	COMSOL Multiphysics [64]

CFD—computational fluid dynamics

formation, interfacial side reactions, volume change, and low coulombic efficiency [61]. Fig. 3 depicts the dominant aging mechanisms at graphite anode. Cathode degradation is discussed in the next subsection.

2.2. Cathode degradation

Recent studies [62] suggest that active cathode material loss also plays a vital role in the battery's degradation process. Causes of cathode degradation include deactivation of active materials due to changes in particle's surface structure and the electronic disconnection between the active materials and a current collector [62]. Further, the cathode material loss due to the DISs [63] also aids the degradation process. These stresses lead to the formation of cracks and an inactive layer on the surface of the cathode, referred to as cathode electrolyte interface (CEI), which leads to LLI.

The evolution of the cracks on the cathode are discussed in [64,65]. The electrode performance was found to be fading due to the fatigue caused by alternating tensile and compressive stresses during the lithiation and delithiation cycles of the battery, respectively. It is found that the non-uniform intercalation and de-intercalation currents also cause stress between the particles in the electrode. In another effort [64], the evolution of stress and strain energy inside the cathode is investigated analytically by integrating the electrochemistry and mechanics. It is observed from the multi-scale mechanical-electrochemical model [64] that an electrochemically inoperative region in an electrode causes stress built-up. The model also addresses the issues arising due to fracture in the cathode.

On the other hand, the quantitative relationship between stress and cathode material loss is studied in [66] along with the influence of other side reactions, such as Li-plating and SEI layer formations. The authors proposed a coupled electrochemical-mechanical-thermal degradation model to include the effects of external factors such as C_{rate} and ambient temperature. A similar detailed non-invasive investigation on the complex interaction between cathode dissolution, CEI growth, particle cracking in both anode and cathode, and SEI growth to understand the aging behavior of the batteries is given in [67].

A summary of all the internal degradation mechanisms discussed above and the softwares used for their modeling approaches are given in Table 4. It can be concluded that mechanical degradation (fracture), Li plating, and cathode degradation contribute to the battery's capacity fade. SEI growth is responsible for both capacity and power fade. Apart from dissecting and relating the internal degradation mechanisms to SOH, it is also necessary to reflect the external factor's contribution to capacity fade and resistance rise in LIBs. The effects of different external aging factors on SOH metrics are discussed in the next section.

3. External factors affecting the degradation of the battery

Degradation of the battery occurs in every stage of its life in different proportions with usage and external operating conditions. Battery degradation can be classified into cycle aging and calendar aging [8]. The calendar-aging corresponds to the consequence of battery storage and cycle-aging is associated with the usage. Battery temperature, charge/discharge rate, depth of discharge (DOD), time, voltage effects during cycling, and SOC during rest periods are the major factors [10] for battery aging. All the above external aging factors responsible for Li loss and increased inner resistance are discussed independently in the next subsections.

3.1. Effect of charging/discharging rate (C_{rate}) and temperature

C_{rate} is defined as the charge/discharge rate at which the battery is cycled. Studies on the influence of charging C_{rate} and cut-off voltages on the aging of batteries are presented in [78,79]. In both these studies charging current has been shown as the deciding factor of LAM, during which the crystal structures of the active material are easily fatigued and damaged. High charging C_{rate} also leads to Li-plating on the anode [80]. Similarly, the discharge capacity significantly falls at a higher discharge rate [81,82]. The degradation mechanisms at a high discharge rate is similar to the ones at high charge rate.

The temperature (T) dependency of aging is, in general, described by the Arrhenius equation and studied in the vast amount of literature [83–87], given by

$$\overline{k}_1 = \overline{k}_0 e^{\frac{-E_a}{R_g T}} \tag{14}$$

where $\overline{k}_0$ is a rate constant, and $\overline{k}_1$ is kinetic reaction rate. Despite a temporary increase in the battery's performance at high temperatures, there is an occurrence of secondary side reactions in terms of corrosion inside the battery. This corrosion degrades the battery faster with LLI, causing capacity fade. High temperatures also cause thickening of SEI film and degradation of the cathode [88], resulting in increased power fade (resistance rise). In [84], the authors found that the Warburg elements and cell impedance increased with cycling at a higher temperatures, but they did not significantly affect the SOH. In real-life applications, temperature fluctuations combined with the discharge rate have a cumulative effect on the battery's capacity fade.

On the other hand, low temperature [89] conditions engender loss of material diffusion and alter the battery chemistry. During low-temperature charging, issues, such as Li plating, dendrite growth, and damage to the crystal structure of active material are reported [47,88,90] due to the high polarization of the anode. This further leads to a significant drop in efficiency at high discharge rates, adversely affecting the SOC and SOH.

3.2. Effect of depth of discharge, state of charge, time, and voltage

Cycle depth or depth of discharge (DOD) is a critical degradation governing factor. DOD is defined as the ratio of the amount of charge released to the battery's nominal capacity. The battery's cycle life reduces at high DOD due to severe structural and volumetric changes leading to LAM. Thus, deep cycles cause disproportional or exponential aging [91,92] than small cycle depths [93]. The influence of DOD on the cycle performance of LIB also varies with different cathode materials [91].

The SOC variation, i.e., change of SOC (ΔSOC), significantly affects aging during cycling. The power loss increases as ΔSOC value is high [94]. At high SOC, i.e., at higher terminal voltages, the SEI layer thickens with the electrolyte decomposition and Li-ion deposition, leading to a higher aging rate [95]. The combination of high SOC and low temperature charging also accelerates the aging phenomenon as a non-linear function of time [96] with the occurrence of Li-ion deposition side reaction. On the other hand, low SOC causes corrosion of anode copper current collectors and structural disordering of cathode active material dramatically, leading to accelerated aging of LIB [97]. Further, batteries exhibit different aging behavior at the same operating temperatures with different SOC levels [44]. It is concluded that the cycling between 45% and 55% SOC has the smallest effect on both capacity loss and resistance increase [96].

Storage time also plays a critical role in battery degradation. The calendar-aging is, in general, due to SEI formation in a carbon-based anode [7,98]. As discussed in the previous section, SEI growth increases the internal resistance. As the SEI thickness grows with aging [25,42]), the power fade increases. In some of the earlier works, this aging processes was linear with respect to time [99]. In later studies, the SEI growth rate is found to be a function of the square root of time ($\sqrt{t}$) [100]. This $\sqrt{t}$ dependency usually represents the incremental capacity loss (ICL) due to SEI growth and is often governed by the diffusion process.

Nonetheless, the charging and discharging voltages impact the battery's aging phenomenon with more capacity degradation and resistance increase [78]. High cathode voltages cause electrolyte oxidation and

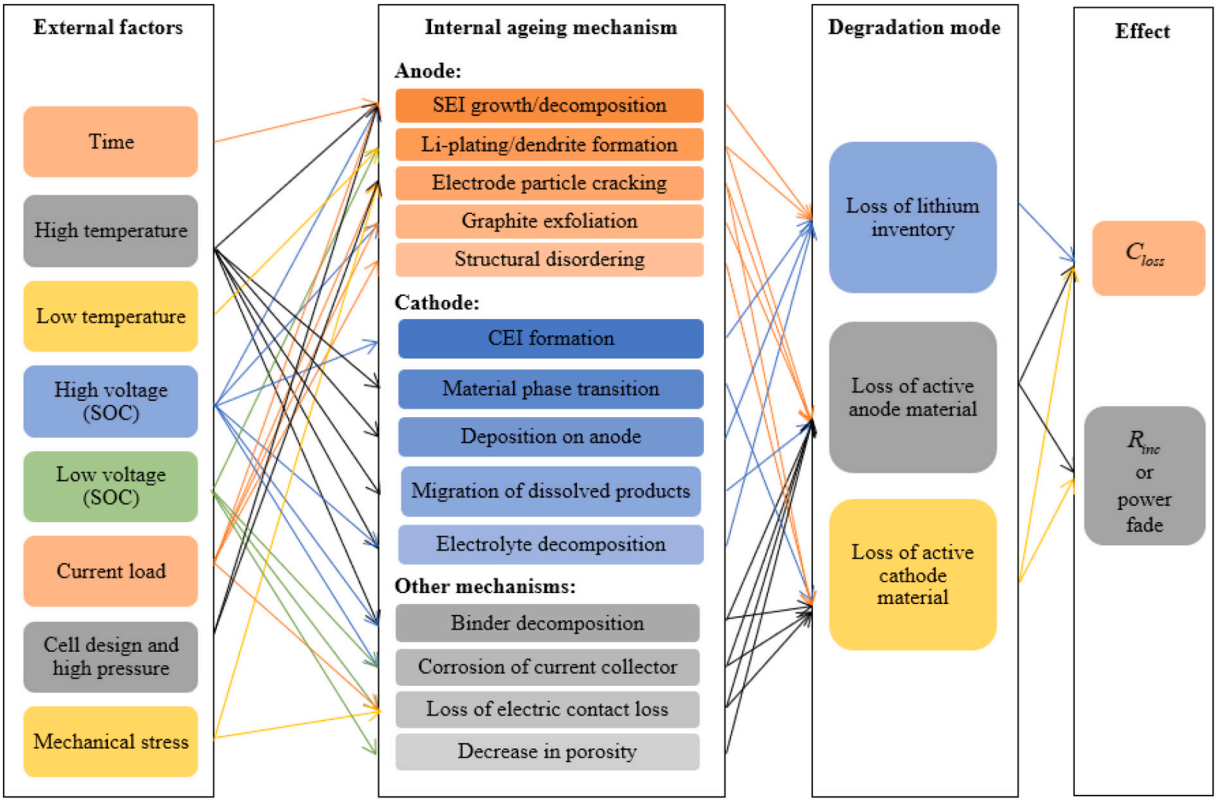

Fig. 4. Cause and effect of degradation mechanisms adapted from [19], where CEI is cathode electrolyte interface, SEI is solid electrolyte interface, SOC is state of charge.

cathode decomposition [101]. On the other hand, low cathode potentials retards the accelerated aging of the battery. In [78], the authors discussed the impact of reducing cut-off voltage on retarded capacity loss and LLI of LIB. A high or low operating voltage window (ΔV) is also shown to affect the aging mechanisms inside the battery [102]. High ΔV causes the LAM of graphite anode, and low ΔV results in high discharge cut-off voltages and irreversible structural changes to graphite anode.

Other factors, such as external abuse, mechanical [74] stress, pressure [103], and choice of the anode, cathode, and electrolyte [104,105], cause the formation, growth, and thickening of the SEI layer accelerating the aging in LIBs. In summary, high/low temperatures, high C_{rates}, high SOC, and ΔV are the common external aging factors of LIB [102]. A cause and effect diagram for the health degradation of LIBs discussed above is shown in Fig. 4. The SOH estimation processes, in regards to the above internal and external degradation mechanisms, is discussed in the next section.

4. SOH estimation methods

The SOH is quantified using two metrics, namely the capacity fade and power fade. Capacity fade is defined as the ratio of current capacity to the nominal/rated capacity (C_{rated}) of the battery [96]. The resistance rise (R_{0inc}) is used as the indicator of power fade and is expressed as

$$R_{0_{inc}} = \frac{R_{bat} - R_{BOL}}{R_{BOL}} \tag{15}$$

where R_{BOL} is the beginning of life resistance, and R_{bat} is the current resistance of the battery. From Eq. (15), the SOH is quantified as,

$$SOH\% = \left(\frac{R_{EOL} - R_{bat}}{R_{EOL} - R_{BOL}}\right) 100\% \tag{16}$$

where R_{EOL} is battery end of life (EOL) internal resistance. The changes in these metrics are caused by both external and internal degradation mechanisms and age. SOH is a multivariate function of these degradation mechanisms making the estimation a challenging task. Since the SOH cannot be measured directly, it is, in general, estimated using various filtering-based approaches. The SOH estimation schemes can be broadly classified as 1) experimental, 2) model-based, and 3) data-driven methods.

Experimental methods constitute of direct/indirect measurement-based approaches. The SOH is estimated by correlating these physical measurements to the properties of the battery. The large test/measurement time preclude the real-time implementation of the experimental methods in BMS. Model-based methods, on the other hand, overcome these limitations and improve the accuracy of SOH estimation by considering the effects of both internal and external aging factors. As discussed above in Section 2, obtaining an accurate model is often challenging. Therefore, data-driven methods, such as analytical and machine learning, were also proposed, which use a large amount of experimental data for learning the black-box model of the battery to estimate and predict SOH.

There are a significant amount of reviews available in the literature (refer to [8–11,15–17], and the references therein) on the above SOH estimation approaches. Unlike the existing reviews, our focus, in this section, is to present a survey of the SOH estimation methods that incorporates studies on different aging mechanisms, discussed in Sections 2 and 3, and the recently developed machine learning-based approaches. The primary goal is to identify future trends and directions in health-conscious intelligent battery management for LIB's safety, longevity, and autonomy.

4.1. Experimental methods

To circumvent the issue of time-intensive tests and measurements for OCV based SOH estimation schemes [106], incremental capacity

analysis (ICA) [107] and differential voltage analysis (DVA) [108] techniques are introduced. The ICA and DVA approaches examines the OCV variations to track the internal chemical reactions and aging mechanisms. These approaches analyze cell voltage responses in different duty regimes, which is the key to understand cell behavior and degradation. The gradient of the capacity with respect to the voltage ($\frac{dC_n}{dOCV}$) defines the incremental capacity (IC), whereas gradient of voltage with respect to capacity, i.e., $\frac{dOCV}{dC_n}$ defines the differential voltage (DV) [109]. The voltage plateaus in the OCV curves are converted to recognizable peaks and valleys in ICA and DVA, respectively. The valleys in the DV curve represent the phase transitions of the electrode active material, while a peak indicates a single phase of the active material.

The influence of external aging factors (DOD, SOC, C_{rate}) on aging are identified by ICA [110] and DVA [111] through four main observations [112]: a) simultaneous decrease of all peaks, b) voltage shift of the peaks, c) decrease of a specific peak, and d) new peaks arising. As discussed in Section 3, these observations can be correlated to the four main degradation modes: LLI [113], LAM_{anode} [110], $LAM_{cathode}$ [114], and degree of lithiation [111]. A systematic approach to identify LIB degradation modes, based on the ICA by analyzing their corresponding IC and peak area main features is presented in [115].

Studies on identification of degradation modes leading to capacity loss are presented in [110,113,116–119]. The IC curves are used to identify two stage capacity loss, which are caused by LAM on both anode and a cathode [116], whereas the DVA is used to find the side reactions on anode [117]. Furthermore, [120] illustrates the correlation between capacity loss and DV curves at different SOC levels, cycling and storage conditions for real-time BMS implementation. The effects of charge/discharge rate and DOD are included in [110,118] for effective SOH estimation with lesser computational load. In [110] the linear relationship between IC peak and remaining capacity is used to provide a quantitative correlation between peak value and the SOH of the LIB. ICA and DVA are also employed to extract parameters, such as LLI and LAM, from the IC and DV curves to establish the multi indicators system of SOH [113,119].

All the above analysis used capacity as a health factor for SOH evaluation. The authors in [121] combined DVA and alternating current impedance to analyze increase of ohmic and polarization resistance (power fade). The increase of ohmic resistance is attributed to the lack of electrolyte and increased separator resistance. SEI layer growth and deterioration of the ionic kinetics result in polarization resistance growth. A similar model-free SOH calculation method by fusion of coulomb counting method and DVA is proposed in [122]. The authors in [123] explore the aging behavior of LIB module using electro impedance spectroscopy (EIS), charge/discharge curve, ICA and average Fréchet distance (AFD). Increase in internal resistance is employed the as health metric. Other similar SOH estimation using ICA and DVA analysis are presented in [107,108,124,125]. Although, ICA and DVA are used for online SOH estimation [107,113,126], these curves are susceptible to measurement noise [118], they require a constant and low current to discharge the battery, and ICA/DVA can only be used under a fully charged/discharged process.

4.2. Model-based SOH estimation with internal degradation

In model-based schemes, the battery physics-based models, i.e., electrochemical, thermal [127], equivalent circuit model (ECM), and their combinations [128], along with degradation models are used to design filters (KF, extended KF, SPF, unscented KF) and/or observers (Luenberger, sliding mode, and nonlinear) to estimate the SOH. These models can be implemented in a wide range of operating conditions and can provide accurate battery behavior and internal parameter changes.

In recent times, the SOH is estimated more accurately by integrating the internal degradation models, discussed in Section 2, with electrochemical models of the LIB. Although SP models are the most commonly used electrochemical models, they do not consider the concentration and potential distribution in the electrolyte phase costing the model's accuracy at high C_{rate}. To overcome this limitation, an advanced SP model is proposed in [129] by considering the electrolyte physics of the battery. Later, the advanced SP model in [129] is adopted by [42] to integrate a capacity degradation model with chemical and mechanical degradation, i.e., SEI layer formation coupled with crack propagation. This integrated model can predict battery capacity loss (C_{loss}) as a function of cycle number and temperature, including SEI layer growth coupled with mechanical fatigue. The capacity loss (LLI) is analyzed in four stages [71] of the SEI layer's evolution under chemical and mechanical stress, such as 1) SEI layer's initial formation, 2) growth of the initially formed SEI layer, 3) SEI layer formation on newly formed surfaces due to fracture/cracking, and 4) growth of the new SEI layers on the fractured surfaces.

The advanced SP models in [42,129] are further reduced and simplified in [130] for online SOH estimation in BMS. This new SP-based comprehensive degradation model includes degradation physics of both anode (coupled chemical/mechanical degradation) and cathode (metal dissolution), and could predict cycling capacity with less than 2% error. The degradation model can also address two main requirements for model-based BMS, i.e., rapid and accurate battery response prediction. On the other hand, a simplified P2D electrochemical model [131] considering side reactions, such as LLI and LAM, is also proposed for SOH prediction. The OCV-SOC relation is updated by integrating the aging effects and is applied to ECM-based SOC estimator. This OCV-SOC correlation is further utilized as a link between ECM and the electrochemical model. The equilibrium potentials are then used to monitor SOH.

Further, for SOH prediction under various operating temperatures, two types of electrochemical models (P2D and SP) are presented in [132] along with degradation models, such as SEI and Li plating. The side reactions are coupled with reduced order P2D for the anode and SP model for the cathode. Here, particle filter (PF) is used to estimate aging parameters as a function of time and electrode thickness and SOH with respect to capacity and power fade in real-time. The aging of the battery is also analyzed at different temperatures, C_{rate} and current profiles. Similarly, the anode SEI growth aging model is coupled with the SPM in [133] to predict the capacity fade of LFP cells with 1.3% error. The operating range of the aging formula at different temperature and SOC is also determined. However, several other degradation mechanisms (fracture, cathode degradation) are yet to be integrated with these electrochemical models.

In addition, ECM models integrated with empirical aging models (refer to Section 4.3.1) are also proposed to predict battery performance under various operating conditions. In [134], an ECM model that integrates the electrical, thermal, and aging aspects of a NMC battery [135] is proposed to estimate SOH. An empirical model is proposed in [136] to predict the voltage profiles of an LFP battery cell at various SOH, SOC, and temperature conditions. Similar electrical-thermal-aging models are employed in [137,138] to develop health conscious optimal battery charging algorithms. A mechanistic model that can synthesize a variety of cell aging scenarios based on degradation modes is presented in [114] with the wide applicability to various cell chemistries, designs, and operating modes. The model consists of a modified ECM capable of simulating the different degradation modes via a synthetic approach based on the behavior of electrodes reflected by the study of the DV and IC curves. The model is also able to simulate complicated degradation modes at any C_{rate} and predict capacity loss, EOL, SOC, IC and DV signatures, without any ambiguity.

4.3. Data-driven methods

Data-driven methods have recently become a research hot spot for their ability to estimate the SOH without the knowledge of electrochemical reaction, explicit physics-based battery model, and physics of

Table 5
Summary of empirical models for capacity and power fade of LIB with different cathode chemistry.

Calendar aging	Cycle aging
Type of cathode used: NMC [96]	Type of cathode used: NMC [96]
$C_{calloss} = \left((7.543V_t - 23.75)10^6 e^{-\frac{6976}{T}}\right)t^{0.75}$	$C_{cycloss} = (7.348\times10^{-3}(\varnothing V_t - 3.667)^2 + 7.600\times10^{-4} + 4.081\times10^{-3}\Delta\text{DOD})\sqrt{Ah}$
$R_{calinc} = \left((5.270V_t - 16.32)10^5 e^{-\frac{5986}{T}}\right)t^{0.75}$	$R_{cycinc} = (2.153\times10^{-4}(\varnothing V_t - 3.725)^2 - 1.521\times10^{-5} + 2.798\times10^{-4}\Delta\text{DOD})\sqrt{Ah}$
Type of cathode used: NMC pouch cell [135]	Type of cathode used: NMC-LMO cathodes [139]
$C_{calloss} = \left(-0.0064\times1.1484^{\frac{V_t - V_0}{\Delta V_t}}\times1.5479^{\frac{T-T_0}{\Delta T}}\right)t^{0.5}$	$C_{cycloss} = a_{cyc}(\text{SOC})e^{\left(\frac{-E_{ac}}{R_g T}\right)}Ah^{0.48}$
$R_{calinc} = \left(0.0484\times1.0670^{\frac{V_t - V_0}{\Delta V_t}}\times1.5665^{\frac{T-T_0}{\Delta T}}\right)t^{0.5}$	$R_{cycinc} = a_{Rcyc}(\text{SOC}, C_{rate})e^{\left(\frac{-E_{aR}}{R_g T}\right)}Ah$
Type of cathode used: LFP [145]	Type of cathode used: LFP [144]
$C_{calloss} = a_{cal}(T,\text{SOC})\left(1+\frac{C_{calloss}(t)}{C_{rated}}\right)^{-\alpha(T)}$	$C_{cycloss} = (-5.31\times10^{-5} + 8.36\times10^{-6}\Delta\text{SOC} + 2.69\times10^{-8}e^{C_{rate}})\times nc^{1.36}$
Type of cathode used: Nano phosphate LFP [141]	Type of cathode used: Nano phosphate LFP [141]
$C_{calloss} = (0.019SOC^{0.823} + 0.5195)\times(3.258\times10^{-9}T^{5.087} + 0.295)\times t^{0.8}$	$C_{cycloss} = (0.00024e^{0.02717T})\times0.02982\times\text{DOD}^{0.4904}\times nc^{0.5}$
$P_{calfade} = \left(\frac{0.000375SOC + 0.1363}{0.155}\right)0.003738e^{0.06778T}t$	$P_{cycfade} = \frac{1}{3}(5.78\times10^{-4}e^{0.03T} + 1.22\times10^{-7})2.918\times10^{-5}e^{0.08657DOD}\times nc^{(0.00434T - 0.008DOD - 0.1504)}$
Type of cathode used: LFP [142]	Type of cathode used: LFP [142]
$C_{calloss} = 3.087\times10^{-7}e^{0.05146T}t^{0.5}$	$C_{cycloss} = 6.87\times10^{-5}e^{0.027T}nc^{0.5}$
$PPC_{caldec} = 1.71\times10^{-29}e^{0.195T}t^{-0.026T+9.85}$	$PPC_{cycdec} = 3.24\times10^{-5}e^{0.03T}nc^{0.00434T-0.65}$
Type of cathode used: LFP [143]	Type of cathode used: LFP [140]
$R_{calinc} = 6.9656\times10^{-8}e^{0.05022T}2.987e^{0.006614SOC}t^{0.8}$	$C_{cycloss} = 30330\times e^{\frac{-31700 + 370.3C_{rate}}{R_g T}}\times Ah^{0.55}$

Note: $C_{calloss}$, and $C_{cycloss}$ in % represent capacity loss during calendar and cycle aging respectively, R_{calinc}, and R_{cycinc} in % represent resistance increase during calendar and cycle aging respectively, $P_{calfade}$, and $P_{cycfade}$ in % represent power fade during calendar and cycle aging respectively, PPC_{caldec}, and PPC_{cycdec} in % represent pulse power capability decrease during discharge pulse during calendar and cycle aging respectively, nc is number of cycles, ΔV_t is change in voltage (V_t), V_0 is initial/reference voltage, ΔT is change in temperature, T_0 is initial/reference temperature, ΔDOD is the depth of discharge or cycle depth in the range of $(0-1)$, ΔSOC is the state of charge in the range of $(0-1)$, E_{ac} is the cell activation energy defined for the capacity fade process, E_{aR} is the cell activation energy, defined for the resistance increase process, fitting parameters of the $a_{cyc}(.)$ and $a_{Rcyc}(.)$ are given in [139], a_{cal} is the kinetic dependence of the capacity fade evolution with T, SOC is given in [145], $\left(1+\frac{C_{calloss}(t)}{C_{rated}}\right)^{-\alpha(T)}$ with $\alpha(T)>0$ is given in [145] which can be related to the diffusion limitation of solvent molecule inside SEI layer which tends to decrease the capacity fade rate. $Li(NiMnCo)O_2$=NMC cathode, $LiFePo_4$= LFP cathode, $NMC - L_iMn_2O_4(LMO)$= NMC-LMO blended cathodes.

the failure mechanism. Unlike model-based methods, data-driven methods depend only on aging data and are discussed in detail in the following subsections.

4.3.1. Analytical methods

Analytical models correlate the aging of a battery with the operation time [18]. These models use capacity loss and power loss as SOH metrics for modeling. Most of these models represent C_{loss} and R_{0inc} as a function of SOC, Ah, and T [139] and is expressed as,

$$C_{loss}(Ah, \text{SOC}, T) = h_c(\text{SOC}, T).Ah^{z_1} \tag{17}$$

where $z_1 = 0.48$, $Ah = C_n \times cycle_{number} \times \text{DOD}$ [140]. At each C_{rate}, Ah is directly proportional to time, so instead of using t as a variable in Eq. (17), Ah is used to quantify and correlate the capacity fading behaviors for different C_{rate}. The function $h_c(.)$ is a non-linear capacity severity function, which depends on the aging factors and C_{rate} (only at high charge/discharge rates) [139] and represented by

$$h_c() = a_c(\text{SOC})e^{\left(\frac{-E_{ac}}{R_g T}\right)} \tag{18}$$

where E_{ac} is the cell activation energy defined for the capacity fade process. The fitting parameters of the $a_c(.)$ are given in [139].

Similarly, the increase in internal resistance $R_{0_{inc}}$ (power fade) as a function of charge throughput is expressed as

$$R_{0_{inc}}(Ah, \text{SOC}, C_{rate}, T) = h_R(\text{SOC}, C_{rate}, T)Ah \tag{19}$$

where $h_R(.)$ is a non-linear resistance severity function that depends on the aging factors as investigated in [139] and is given by

$$h_R() = a_R(\text{SOC}, C_{rate})e^{\left(\frac{-E_{aR}}{R_g T}\right)} \tag{20}$$

where E_{aR} is the cell activation energy, defined for the resistance increase process. The fitting parameters of the $a_R(.)$ are detailed in [139].

A summary of empirical models for capacity and power fade of LIB with different cathode chemistry developed with extensive experimentation under controlled environments [96,135,139–144] is presented in Table 5. The table presents the analytical life-cycle models for two commonly used battery chemistry, i.e., LFP and NMC. In both LFP [140] and NMC [139] batteries, the effect of temperature in cycle-life models is obtained using Arrhenius correlation and power law relation with time or Ah.

It is well known that the LFP cathode cells present better durability, inherent safety, and rely on abundant, eco-friendly materials [146]. However, the major limitations of LFP cells are low specific energy and dramatic changes in OCV-SOC curve, as the SOCs drop to 0% and rise to 100%, and wide flat OCV plateau in the middle SOC regions. Therefore, the cycle-aging for LFP [142,144] are found to vary with the number of cycles (nc). Compared to LFP cells, aging in NMC cells [96,135] includes the effect of storage voltage, time, and temperature during calendar-

aging and DOD, SOC, C_{rate} and Ah for cycle-aging. Note that the NMC batteries, discussed in Table 5, constitute pouch cells instead of cylindrical cells. The primary limitation of all the semi-empirical models presented in Table 5 is that they don't reflect the contributions of the internal degradation mechanisms explicitly in the expressions.

Recent studies [147–150] consider a subset of the degradation mechanisms (e.g., SEI formation and growth) to represent analytical aging models. Three semi-empirical models of the three aging modes (LLI, LAM_{anode},$LAM_{cathode}$) are quantified by the established OCV model in [149], along with the development of the mapping models with SOH, ohmic resistance and polarization resistance evolution. The authors, established a clear mapping from external stress to internal aging mechanism to external behavior. Although several empirical methods based on the DV curve have been proposed in [120,126], the features used to estimate the capacity are sensitive to the relatively high initial SOC and charging current, which was redressed in [150]. However, in [150] the correlations between the extracted features and battery aging mechanisms, such as the LLI, LAM_{anode}, and $LAM_{cathode}$ are not completely elucidated, especially for the battery with NMC cathode. Later, the authors in [113] extracted six characteristic parameters revealing LAM_{anode}, and $LAM_{cathode}$ and LLI from the IC curve to establish the multi-indicators system describing battery SOH for NMC LIB, which enables ICA to be used in on-board applications. In addition, LLI is found to be the dominant factor causing capacity loss for battery under 20% DOD.

4.3.2. Machine learning methods

Machine learning approaches use the SOH data to fit a model, which can be used for future prediction. The machine learning methods used for SOH estimation are artificial neural networks (ANN) [151,152], SVM [153–155], and fuzzy logic [156,157]. ANN is one of the approximation methods, which can fit complex non-linear functions. In [152], a robust algorithm for ANN is presented, predicting SOH at different operating conditions. However, the main limitation of ANNs include the requirement of a large amount of training data and the training method, which significantly affect the accuracy. Furthermore, the identification and optimization of the model topology of ANN remain an open technical challenge [18]. Other probabilistic approaches, such as Gaussian process regression (GPR) [158], relevant vector machine (RVM) [159] are also used in literature to estimate the SOH of the battery. However, the above methods are mostly affected by the phenomenon of capacity regeneration and cannot make long-term predictions. Recently, deep learning became popular in battery health prediction due to its powerful ability to achieve accurate long-term degradation predictions [160].

Deep NNs (DNN), convolutional NNs (CNN) and recurrent NNs (RNN) are introduced for system modeling, time series forecasting, and natural language processing [161]. These deep learning technologies eliminate the need for data labeling and feature engineering by extracting higher-level features from input data using multiple layers. Recent studies [161–163] have reported using these technologies to establish a relationship between the features of battery degradation from the battery characterization data and the SOH of the battery. In [162], a deep CNN is used to estimate the capacity of a battery, whose unique features include the local connectivity and shared weights. A similar investigation on models of three different families of NN architectures, such as feed-forward NN (FNN), CNN, and long short-term memory NN (LSTMNN) are proposed in [163] for battery capacity estimation. LSTMNN is found to outperform other model architectures in estimating battery capacity more accurately because of its simpler structure and its ability to interpret variable sized time-series battery data in an efficient manner. On the other hand, in [161] a two stream hybrid gate recurrent unit (GRU)-CNN is employed to build a time series prediction problem for SOH estimation. All these studies use voltage, current, temperature during the charging as inputs to learn the model and predict the SOH of the battery with good accuracy. In all the above techniques future capacity values are predicted based on the trained model until the capacity reaches the EOL (20% capacity loss).

In real-time applications, it is difficult to measure battery capacity directly due to incomplete discharge. In addition identifying internal aging mechanisms inducing capacity/power fade through data-driven methods is cumbersome. Therefore, some health indicators (HIs) are extracted from the measured parameters (voltage, current, temperature, and time interval) to estimate SOH using data-driven approaches. They are especially important for the data-driven methods as battery internal

Table 6
A comparison of emerging SOH estimation methods.

Methods	References	Key benefits	Limitations	Accuracy
Data-driven approach	[151,152]	Simple structure, easy to identify parameters, easy to implement, strong ability to consider nonlinearities, high prediction accuracy, non-parametric, robust to outliers, low prediction time.	Easy to cause under-fitting problems due to its linear regression type, potential overfitting problems, poor generalization ability, bad long-term prediction ability, poor uncertainty management ability, performance highly depends on the training process.	RMSE ≈ 0.0203
Hybrid methods	[175,178]	Prediction accuracy is high and avoids the estimation error from the model mismatch, and enhances the model's adaptability to varying operating condition.	Computation is complicated and depends on experimental data, restricts its applicability under more complex aging conditions when combined with model-based methods.	MARE ≈ 0.27%,RMSE ≈ 0.0037
Empirical methods	[141,143]	Easy to be built up and quick to produce predictions, simple structure easy of extracting model parameters, the low computational effort.	Extensive laboratory tests over the entire operating range are required, poor robustness, low accuracy, difficult to develop suitable laboratory aging tests to analyze the interaction between different aging processes and link them to life expectancy on an experimental basis, low generalizability, and developed models are restricted to a specific battery type and operating conditions.	R^2 ≈ 0.963, ARE ≈ 9.72%
Physics-based models	[37,66]	High accuracy, linked to the underlying physics of the battery.	Heavy computation load, difficult model parameterization.	RMSE ≈ 0.002
DVA/ICA based methods	[109,110]	Easy to monitor and implement in BMS for online applications, indicative of the intercalation process.	Limited to low current rates, sensitive to measurement noise and temperature, heavy data requirements of voltage and current measurements.	ME ≈ 4%, RMSE ≈ 6.4
Physics-based degradation mechanisms + Big data	[179,180]	Highly accurate, implementable in online BMS applications, vast quantities of data are processed and treated with high accuracy at the same time.	It needs a large amount of data to train and the accuracy depends on the model used.	RMSE ≈ 5%
Deep neural network	[161,163]	Automates the feature learning process from the large amounts of data, learn highly representative features that carry the most useful information of the data	It needs a large amount of data to train.	ME ≈ 4.3%, RMSE ≈ 4.69%

RMSE—root mean square error, MARE—mean absolute relative error, ARE—average relative estimation error, ME—maximum estimation error.

aging mechanisms are known to be manifested by these HIs [164]. A novel method to predict RUL based on the optimized health indicators and online model correction with transfer learning is presented in [160]. GPR is used to optimize the threshold for HIs and determine the end of life of LIB. The SOH of the battery is evaluated using grey relational analysis (GRA) in [109]. The HIs were extracted from the partial IC curves for GRA. A voltage-temperature health feature extraction method for batteries is proposed in [165]. Another approach using partial voltage profiles and GPR is also proposed to extract voltage-dependent health features. In [166] HIs are extracted to estimate the SOH under general discharging conditions, such as CC, pulse current, and dynamic current and using these HIs as input features linear regression (LR), SVM, RVM, and GPR, are employed to predict the SOH of the battery. Recent studies [164,167] also include significant dimensional reduction of HIs. A HIs extraction and optimization using IC curves is presented in [164]. An improved GPR is applied for battery capacity estimation.

In recent times, hybrid methods [168], which combine similar or different methods, have also become the main research focus to improve SOH estimation and RUL prediction. Hybrid data-driven and model-based approaches are two notable ones [169–172]. In [173], an aging phenomenon, based on the rain-flow cycle counting method combined with deep-learning algorithm is presented. This hybrid method extracts the battery aging trajectory and provide an aging index to improve the SOH estimation accuracy. Ensemble of data-driven strategies are also proposed [109,174–177] to further improve the accuracy and reduce the computational load. A comparison of all the emerging SOH estimation methods along with their accuracy is given in Table 6. We can observe that hybrid approaches are compelling, more accurate and reliable for SOH estimation of LIBs.

In the next section, we summarize the above studies and provide recommendations for future research direction to develop intelligent BMSs with health-conscious decision-making capabilities.

5. Discussion and future recommendations

From the above studies, the internal degradation steps starting from SEI formation to lithium plating can be summarized as follows: 1) SEI layer grows in width substantially at the anode with consecutive charge and discharge cycles. 2) Due to SEI's permeability to Li-ions, large stresses are generated leading to fractures of electrodes. 3) SEI layer formation and its growth lead to reduction in anode's porosity, which further results in Li-plating or Li-metal formation at the narrow gap between the anode and the electrolyte. 4) Li-plating again results in protrusions on electrode surface leading to dendrites. It is well established that the dominant aging mechanisms for graphite anode LIBs are SEI formation, which increases the impedance and the consumption of Li ions [181]. Additionally, lithium metal plating could also contribute to accelerated aging, causing further increase in capacity and power fade. It can be concluded that while the fracture, lithium plating, and dendrite formation leads to loss of active lithium resulting in capacity loss, the SEI layer formation affects both the capacity loss and power fade. On the other hand cathode materials in LIBs are significantly affected by both cycling and calendar life. The characteristics of cathode may differ from one chemistry to another due to their sensitivities to aging. Thus, the degradation mechanisms can be clustered into LLI, LAM_{anode}, $LAM_{cathode}$ and increase of the faradic and ohmic resistances [19].

Capacity loss is caused by LAM and LLI, and recent studies [182] have shown that LLI is prominent when compared to LAM. LLI is caused due to irreversible Li-plating and SEI layer formation and its growth [21]. Li-ions are inclined to form metallic Li at low temperatures which decreases the amount of cyclable Li-ions that manifests itself as capacity loss. Consequently low temperature charging accelerates the aging phenomenon of LIB [96]. Although, Li-plating can be reduced by optimized charging process [183], SEI formation and its growth is prudent and also unavoidable. While, LLI can take place alone, LAM takes place simultaneously with LLI [115] and lead to both capacity and power fade. LAM can originate from three basic sets of conditions: structural changes during cycling, chemical decomposition or dissolution reactions and surface film modification [120]. On the other hand ohmic resistance increase is the result of various sources of LLI and LAM [115].

It is evident that the modeling and estimation of the above internal degradation processes is complex due to the interplay among these degradation mechanisms. From the perspective of modeling, recent studies on the continuum model [37] and atomistic-scale mechanisms [184] can be a powerful combination for predicting SEI growth and parameters, such as conductivity. Continuum models, which incorporate chemical/electrochemical kinetics and transport phenomena to produce more accurate predictions than empirical models, provide deeper insight into the cell. These models will provide a new perception of structural growth and the transport of ions in the SEI, and need further research.

In recent times, these electrochemical degradation models, discussed in Section 2, are integrated with the electrochemical SP model [37,66,185] for improved SOH estimation. Results on integration of SEI, fracture, cathode dissolution, CEI growth, particle cracking in both anode and cathode for SOH estimation are available in literature [67]. However, several internal degradation mechanisms, such as Li-plating and Li-dendrites, are yet to be integrated while estimating the health of LIB. Although Li-plating on graphite anodes is partly reversible [186], Li dendrite could still form on the graphite anodes during fast charging and overcharging conditions, especially in a long-range electric vehicle [58]. Further, the studies [4,42,48,49] incorporating advanced SP and reduced-order P2D models are partially comprehensive in considering the combination of various degradation mechanisms to understand the aging effects along with predicting C_{loss} of the battery. These integrated model-based approaches for SOH estimation have improved the SOH estimation accuracy significantly, but still in an infant stage and an open area of future research.

External factors, such as high C_{rate}, high SOC, or low temperatures accelerate the battery's degradation [4] by affecting the internal degradation mechanisms, as discussed in Section 3. Analytical aging models [96,135,139,140,147,148] are used to represent the capacity and power fade of the battery under various operating conditions for different battery chemistry, as discussed in Table 5. Semi-empirical aging models, representing the degradation modes of the LIB [149] at different operating conditions, lay the foundations of understanding the interconnection between external stress, internal aging mechanism and external behavior (capacity/power fade). Therefore, several ECMs [134,137,138] are integrated with these analytical models to predict battery's life-cycle performance. The recent efforts, in [187], to use an improved P2D model to obtain a relationship between the ECM electrical and electrochemical parameters suggest SOH-integrated ECM modeling approaches for more reliable, accurate and cost effective solution for SOH estimation, when compared to basic electrochemical models [42]. Integrating or reflecting the contributions of internal degradation mechanisms with empirical models could further improve the SOH estimation results and can be another research direction.

Further, the internal battery parameters, both in electrochemical and ECM, are time-varying. The parameters vary with change in SOC, capacity, and power fade. Therefore, constant parameters ECM, integrated with empirical aging models, lacks the accuracy in SOH estimation. Incorporating parameter varying ECMs for SOC [188] and SOH estimation will further improve the estimation accuracy. Development of filters or learning schemes to estimate/learn the time-varying parameters can provide a more reliable prediction of SOH. However, estimating or learning the time-varying parameters in real-time is a challenging problem and could be an area of future research.

On the other hand, machine-learning-based approaches are gaining interest. Both shallow and deep-learning based approaches are also applied to LIB's SOC and SOH estimation. Recently, deep learning schemes such as CNN, RNN, FNN, GRU-CNN and LSTMNN are used in predicting the SOH of LIB with good accuracy due to their potent capability to make accurate long-term degradation predictions

[160,161]. One of the primary limitations of these machine learning approaches is the unavailability of a large amount of degradation data for implementation. To circumvent the issue of large SOH data, real-time online machine learning-based approaches are promising. The learning schemes must use the online measured data to update the learned models with lesser computation requirements. Further, the recent developments in computationally efficient real-time learning [189,190] in the control research community can be leveraged to learn the complex nonlinear LIB model with reduced computational requirement.

Another alternative to the data hungry machine learning approaches is the hybrid methods, such as ICA-data-driven [109,176], model-based-data-driven [178]), and GPR. These methods are found to be more accurate, compelling, and reliable estimation methods than the traditional learning only algorithms. They have more significant potential, compatibility, and adaptability to varying operating conditions for industrial applications. ICA/DVA methods have also been developed for onboard battery SOC and SOH estimation [191]. Recently, GPR based method is an emerging data-driven approach. It is a Bayesian non-parametric probability approach with remarkable performance in non-linear mapping. The non-parametric GPR-based model is considerably convenient to implement on-board with the support of voltage and temperature measurements [165]. GPR is used to extract HI's which unmasks the battery internal aging mechanisms to estimate the SOH of LIBs [164,166,167]. Unlike other data-driven methods, such as SVM, and ANN, GPR brings statistical thought into machine learning, which helps the approach be more accurate. It is also capable of dealing with issues, such as small sample and prediction uncertainty representation for battery degradation modeling and prognosis [165]. The hybrid approaches are also one of the promising areas of future research for adaptability and autonomy of battery management systems in battery health prediction.

6. Conclusion

In this paper, we have summarized different internal and external degradation mechanisms of LIB, and provided details of the corresponding modeling approaches and correlation with the SOH. More specifically, we systematically presented the evolution of the chemical and mechanical degradation starting from the SEI layer formation, fracture, lithium plating and dendrite formation along with their governing equations. The inter-relations among these degradation mechanisms and their effects on capacity and power fade are also discussed. Although there are several models developed for these internal degradation mechanisms, further research is required to understand the distinguished effects of external degradation inducing factors on these internal degradation mechanisms.

From the SOH estimation perspective, we have presented the recent and advanced SOH estimation methods, such as OCV based ICA-DVA techniques, electrochemical methods integrated with internal degradation models, and data driven methods using DNN, GPR. Further, a summary of empirical models for capacity or power fade, along with the influence of the external aging factors on internal degradation mechanisms are discussed. It is clear from the review that the hybrid approaches, which combine multiple estimation schemes, improve the SOH estimation accuracy. It is also observed that real-time machine learning based approaches are less explored in the area of LIB, and gaining popularity in recent times.

Finally, nondestructive quantitative evaluations of the degradation, taking the impact of internal and external aging factors into account, will result in well-optimized cell designs with longer cycle life. Development of real-time machine learning schemes with measured voltage, current, and surface temperature, by leveraging the advancement in NN based architectures and training schemes, can address the challenges in modeling the internal degradation. Further, these learning based intelligent models can be implemented in BMS for health-conscious decision making with improved autonomy.

CRediT authorship contribution statement

Geetika Vennam (First Author): Conceptualization, Investigation, Writing-Original Draft.

Avimanyu Sahoo (Second Author): Reviewing & editing the manuscript, Research supervision, and Funding acquisition.

Samir Ahmed (Third Author): Reviewing and Funding acquisition.

Declaration of competing interest

The authors declare that they have no known competing financial interests or personal relationships that could have appeared to influence the work reported in this paper.

Acknowledgement

This work was supported by the Transportation Consortium of South-Central States (Tran-SET), Louisiana State University, Baton Rouge (# PO-0000029576).

References

[1] Y. Nishi, Lithium ion secondary batteries; past 10 years and the future, J. Power Sources 100 (1–2) (2001) 101–106.
[2] M. Chen, X. Ma, B. Chen, R. Arsenault, P. Karlson, N. Simon, Y. Wang, Recycling end-of-life electric vehicle lithium-ion batteries, Joule 3 (11) (2019) 2622–2646.
[3] A. Khaligh, M. D'Antonio, Global trends in high-power on-board chargers for electric vehicles, IEEE Trans. Veh. Technol. 68 (4) (2019) 3306–3324.
[4] X.-G. Yang, Y. Leng, G. Zhang, S. Ge, C.-Y. Wang, Modeling of lithium plating induced aging of lithium-ion batteries: transition from linear to nonlinear aging, J. Power Sources 360 (2017) 28–40.
[5] J. Li, J.K. Barillas, C. Guenther, M.A. Danzer, A comparative study of state of charge estimation algorithms for LiFePO4 batteries used in electric vehicles, J. Power Sources 230 (2013) 244–250.
[6] J.K. Barillas, J. Li, C. Günther, M.A. Danzer, A comparative study and validation of state estimation algorithms for Li-ion batteries in battery management systems, Appl. Energy 155 (2015) 455–462.
[7] J. Vetter, P. Novák, M.R. Wagner, C. Veit, K.-C. Möller, J. Besenhard, M. Winter, M. Wohlfahrt-Mehrens, C. Vogler, A. Hammouche, Ageing mechanisms in lithium-ion batteries, J. Power Sources 147 (1–2) (2005) 269–281.
[8] C. Lin, A. Tang, W. Wang, A review of SOH estimation methods in lithium-ion batteries for electric vehicle applications, Energy Procedia 75 (2015) 1920–1925.
[9] J. Zhang, J. Lee, A review on prognostics and health monitoring of li-ion battery, J. Power Sources 196 (15) (2011) 6007–6014.
[10] H. Tian, P. Qin, K. Li, Z. Zhao, A review of the state of health for lithium-ion batteries: research status and suggestions, J. Clean. Prod. 120813 (2020).
[11] L. Lu, X. Han, J. Li, J. Hua, M. Ouyang, A review on the key issues for lithium-ion battery management in electric vehicles, J. Power Sources 226 (2013) 272–288.
[12] M.U. Cuma, T. Koroglu, A comprehensive review on estimation strategies used in hybrid and battery electric vehicles, Renew. Sust. Energ. Rev. 42 (2015) 517–531.
[13] M.-K. Tran, S. Panchal, V. Chauhan, N. Brahmbhatt, A. Mevawalla, R. Fraser, M. Fowler, Python-based scikit-learn machine learning models for thermal and electrical performance prediction of high-capacity lithium-ion battery, Int. J. Energy Res. 46 (2) (2022) 786–794.
[14] J. Qiao, X. Liu, Z. Chen, Prediction of the remaining useful life of lithium-ion batteries based on empirical mode decomposition and deep neural networks, IEEE Access 8 (2020) 42760–42767.
[15] M. Berecibar, I. Gandiaga, I. Villarreal, N. Omar, J. Van Mierlo, P. Van den Bossche, Critical review of state of health estimation methods of li-ion batteries for real applications, Renew. Sust. Energ. Rev. 56 (2016) 572–587.
[16] M.H. Lipu, M. Hannan, A. Hussain, M. Hoque, P.J. Ker, M. Saad, A. Ayob, A review of state of health and remaining useful life estimation methods for lithium-ion battery in electric vehicles: challenges and recommendations, J. Clean. Prod. 205 (2018) 115–133.
[17] R. Xiong, L. Li, J. Tian, Towards a smarter battery management system: a critical review on battery state of health monitoring methods, J. Power Sources 405 (2018) 18–29.
[18] Y. Li, K. Liu, A.M. Foley, A. Zülke, M. Berecibar, E. Nanini-Maury, J. Van Mierlo, H.E. Hoster, Data-driven health estimation and lifetime prediction of lithium-ion batteries: a review, Renew. Sust. Energ. Rev. 113 (2019), 109254.
[19] C.R. Birkl, M.R. Roberts, E. McTurk, P.G. Bruce, D.A. Howey, Degradation diagnostics for lithium ion cells, J. Power Sources 341 (2017) 373–386.
[20] E. Peled, The electrochemical behavior of alkali and alkaline earth metals in nonaqueous battery systems—the solid electrolyte interphase model, J. Electrochem. Soc. 126 (12) (1979) 2047.
[21] C. Uhlmann, J. Illig, M. Ender, R. Schuster, E. Ivers-Tiffée, In situ detection of lithium metal plating on graphite in experimental cells, J. Power Sources 279 (2015) 428–438.

[22] B. Khanal, B. Bahrami, H. Lu, Q. Qiao, Modelling of solid electrolyte interface (SEI) layer of lithium-ion batteries using kinetic monte carlo approach, in: IIE Annual Conference. Proceedings, Institute of Industrial and Systems Engineers (IISE), 2017, pp. 1193–1198.

[23] A. Wang, S. Kadam, H. Li, S. Shi, Y. Qi, Review on modeling of the anode solid electrolyte interphase (SEI) for lithium-ion batteries, npj Comput. Mater. 4 (1) (2018) 1–26.

[24] T.F. Fuller, M. Doyle, J. Newman, Simulation and optimization of the dual lithium ion insertion cell, J. Electrochem. Soc. 141 (1) (1994) 1–10.

[25] J. Christensen, J. Newman, A mathematical model for the lithium-ion negative electrode solid electrolyte interphase, J. Electrochem. Soc. 151 (11) (2004) A1977.

[26] Y. Xie, J. Li, C. Yuan, Multiphysics modeling of lithium ion battery capacity fading process with solid-electrolyte interphase growth by elementary reaction kinetics, J. Power Sources 248 (2014) 172–179.

[27] S. Sankarasubramanian, B. Krishnamurthy, A capacity fade model for lithium-ion batteries including diffusion and kinetics, Electrochim. Acta 70 (2012) 248–254.

[28] L. Liu, M. Zhu, Modeling of SEI layer growth and electrochemical impedance spectroscopy response using a thermal-electrochemical model of li-ion batteries, ECS Trans. 61 (27) (2014) 43.

[29] M. Doyle, T.F. Fuller, J. Newman, Modeling of galvanostatic charge and discharge of the lithium/polymer/insertion cell, J. Electrochem. Soc. 140 (6) (1993) 1526–1533.

[30] P. Ramadass, B. Haran, P.M. Gomadam, R. White, B.N. Popov, Development of first principles capacity fade model for li-ion cells, J. Electrochem. Soc. 151 (2) (2004) A196–A203.

[31] M. Doyle, J. Newman, A.S. Gozdz, C.N. Schmutz, J.-M. Tarascon, Comparison of modeling predictions with experimental data from plastic lithium ion cells, J. Electrochem. Soc. 143 (6) (1996) 1890–1903.

[32] S. Santhanagopalan, Q. Guo, P. Ramadass, R.E. White, Review of models for predicting the cycling performance of lithium ion batteries, J. Power Sources 156 (2) (2006) 620–628.

[33] S. Santhanagopalan, R.E. White, Online estimation of the state of charge of a lithium ion cell, J. Power Sources 161 (2) (2006) 1346–1355.

[34] A.M. Colclasure, R.J. Kee, Thermodynamically consistent modeling of elementary electrochemistry in lithium-ion batteries, Electrochim. Acta 55 (28) (2010) 8960–8973.

[35] F. Single, B. Horstmann, A. Latz, Dynamics and morphology of solid electrolyte interphase (sei), Phys. Chem. Chem. Phys. 18 (27) (2016) 17810–17814.

[36] F. Single, B. Horstmann, A. Latz, Revealing SEI morphology: in-depth analysis of a modeling approach, J. Electrochem. Soc. 164 (11) (2017) E3132.

[37] M. Heinrich, N. Wolff, N. Harting, V. Laue, F. Röder, S. Seitz, U. Krewer, Physico-chemical modeling of a lithium-ion battery: an ageing study with electrochemical impedance spectroscopy, Batteries Supercaps 2 (6) (2019) 530–540.

[38] J. Christensen, J. Newman, A mathematical model of stress generation and fracture in lithium manganese oxide, J. Electrochem. Soc. 153 (6) (2006) A1019.

[39] R. Deshpande, Y. Qi, Y.-T. Cheng, Effects of concentration-dependent elastic modulus on diffusion-induced stresses for battery applications, J. Electrochem. Soc. 157 (8) (2010) A967.

[40] R.D. Deshpande, D.M. Bernardi, Modeling solid-electrolyte interphase (SEI) fracture: coupled mechanical/chemical degradation of the lithium ion battery, J. Electrochem. Soc. 164 (2) (2017) A461.

[41] Q. Deng, R. Hu, C. Xu, B. Chen, J. Zhou, Modeling fracture of solid electrolyte interphase in lithium-ion batteries during cycling, J. Solid State Electrochem. 23 (11) (2019) 2999–3008.

[42] J. Li, K. Adewuyi, N. Lotfi, R. Landers, J. Park, A single particle model with chemical/mechanical degradation physics for lithium ion battery state of health (SOH) estimation, Appl. Energy 212 (2018) 1178–1190.

[43] A. Barré, B. Deguilhem, S. Grolleau, M. Gérard, F. Suard, D. Riu, A review on lithium-ion battery ageing mechanisms and estimations for automotive applications, J. Power Sources 241 (2013) 680–689.

[44] K. Nunotani, F. Yoshida, Y. Kamiya, Y. Daisho, K. Abe, M. Kono, H. Matsuo, Development and performance evaluation of lithium iron phosphate battery with superior rapid charging performance—second report: evaluation of battery capacity loss characteristics, in: 2011 IEEE Vehicle Power and Propulsion Conference, IEEE, 2011, pp. 1–4.

[45] P. Arora, M. Doyle, R.E. White, Mathematical modeling of the lithium deposition overcharge reaction in lithium-ion batteries using carbon-based negative electrodes, J. Electrochem. Soc. 146 (10) (1999) 3543.

[46] R.D. Perkins, A.V. Randall, X. Zhang, G.L. Plett, Controls oriented reduced order modeling of lithium deposition on overcharge, J. Power Sources 209 (2012) 318–325.

[47] H. Ge, T. Aoki, N. Ikeda, S. Suga, T. Isobe, Z. Li, Y. Tabuchi, J. Zhang, Investigating lithium plating in lithium-ion batteries at low temperatures using electrochemical model with nmr assisted parameterization, J. Electrochem. Soc. 164 (6) (2017) A1050.

[48] D. Ren, K. Smith, D. Guo, X. Han, X. Feng, L. Lu, M. Ouyang, J. Li, Investigation of lithium plating-stripping process in li-ion batteries at low temperature using an electrochemical model, J. Electrochem. Soc. 165 (10) (2018) A2167.

[49] X. Zhao, Y. Yin, Y. Hu, S.-Y. Choe, Electrochemical-thermal modeling of lithium plating/stripping of Li(Ni06Mn02Co02)O2/carbon lithium-ion batteries at subzero ambient temperatures, J. Power Sources 418 (2019) 61–73.

[50] L. Chen, B. Liu, A.N. Abbas, Y. Ma, X. Fang, Y. Liu, C. Zhou, Screw-dislocation-driven growth of two-dimensional few-layer and pyramid-like wse2 by sulfur-assisted chemical vapor deposition, ACS Nano 8 (11) (2014) 11543–11551.

[51] J. Luo, C.-E. Wu, L.-Y. Su, S.-S. Huang, C.-C. Fang, Y.-S. Wu, J. Chou, N.-L. Wu, A proof-of-concept graphite anode with a lithium dendrite suppressing polymer coating, J. Power Sources 406 (2018) 63–69.

[52] R. Akolkar, Mathematical model of the dendritic growth during lithium electrodeposition, J. Power Sources 232 (2013) 23–28.

[53] X. Wang, W. Zeng, L. Hong, W. Xu, H. Yang, F. Wang, H. Duan, M. Tang, H. Jiang, Stress-driven lithium dendrite growth mechanism and dendrite mitigation by electroplating on soft substrates, Nat. Energy 3 (3) (2018) 227–235.

[54] C. Monroe, J. Newman, Dendrite growth in lithium/polymer systems: a propagation model for liquid electrolytes under galvanostatic conditions, J. Electrochem. Soc. 150 (10) (2003) A1377.

[55] R. Akolkar, Modeling dendrite growth during lithium electrodeposition at sub-ambient temperature, J. Power Sources 246 (2014) 84–89.

[56] A.K. Sethurajan, J.M. Foster, G. Richardson, S.A. Krachkovskiy, J.D. Bazak, G. R. Goward, B. Protas, Incorporating dendrite growth into continuum models of electrolytes: insights from nmr measurements and inverse modeling, J. Electrochem. Soc. 166 (8) (2019) A1591.

[57] Y. Ren, Y. Zhou, Y. Cao, Inhibit of lithium dendrite growth in solid composite electrolyte by phase-field modeling, The Journal of Physical Chemistry C.

[58] C. Shen, G. Hu, L.-Z. Cheong, S. Huang, J.-G. Zhang, D. Wang, Direct observation of the growth of lithium dendrites on graphite anodes by operando ec-afm, Small Methods 2 (2) (2018), 1700298.

[59] P. Harks, F. Mulder, P. Notten, In situ methods for li-ion battery research: a review of recent developments, J. Power Sources 288 (2015) 92–105.

[60] J. Steiger, D. Kramer, R. Mönig, Microscopic observations of the formation, growth and shrinkage of lithium moss during electrodeposition and dissolution, Electrochim. Acta 136 (2014) 529–536.

[61] Z. Guo, J. Zhu, J. Feng, S. Du, Direct in situ observation and explanation of lithium dendrite of commercial graphite electrodes, RSC Adv. 5 (85) (2015) 69514–69521.

[62] K. Ando, T. Matsuda, D. Imamura, Degradation diagnosis of lithium-ion batteries with a LiNi05Co02Mn03O2 and LiMn2O4 blended cathode using dV/dQ curve analysis, J. Power Sources 390 (2018) 278–285.

[63] R. Xu, H. Sun, L.S. de Vasconcelos, K. Zhao, Mechanical and structural degradation of LiNixMnyCozO2 cathode in Li-ion batteries: an experimental study, J. Electrochem. Soc. 164 (13) (2017) A3333.

[64] B. Wu, W. Lu, A battery model that fully couples mechanics and electrochemistry at both particle and electrode levels by incorporation of particle interaction, J. Power Sources 360 (2017) 360–372.

[65] Y. Zhang, C. Zhao, Z. Guo, Simulation of crack behavior of secondary particles in Li-ion battery electrodes during lithiation/de-lithiation cycles, Int. J. Mech. Sci. 155 (2019) 178–186.

[66] S.-C. Yang, Y. Hua, D. Qiao, Y.-B. Lian, Y.-W. Pan, Y.-L. He, A coupled electrochemical-thermal-mechanical degradation modelling approach for lifetime assessment of lithium-ion batteries, Electrochim. Acta 326 (2019), 134928.

[67] P.S. Sabet, A.J. Warnecke, F. Meier, H. Witzenhausen, E. Martinez-Laserna, D. U. Sauer, Non-invasive yet separate investigation of anode/cathode degradation of lithium-ion batteries (nickel–cobalt–manganese vs. graphite) due to accelerated aging, J. Power Sources 449 (2020), 227369.

[68] K.A. Smith, C.D. Rahn, C.-Y. Wang, Control oriented 1d electrochemical model of lithium ion battery, Energy Convers. Manag. 48 (9) (2007) 2565–2578.

[69] R. Mehta, A. Gupta, An improved single-particle model with electrolyte dynamics for high current applications of lithium-ion cells, Electrochim. Acta 389 (2021), 138623.

[70] W. Mei, Q. Duan, P. Qin, J. Xu, Q. Wang, J. Sun, A three-dimensional electrochemical-mechanical model at the particle level for lithium-ion battery, J. Electrochem. Soc. 166 (14) (2019) A3319.

[71] R. Deshpande, M. Verbrugge, Y.-T. Cheng, J. Wang, P. Liu, Battery cycle life prediction with coupled chemical degradation and fatigue mechanics, J. Electrochem. Soc. 159 (10) (2012) A1730.

[72] I. Laresgoiti, S. Käbitz, M. Ecker, D.U. Sauer, Modeling mechanical degradation in lithium ion batteries during cycling: solid electrolyte interphase fracture, J. Power Sources 300 (2015) 112–122.

[73] C. Miehe, H. Dal, L.-M. Schänzel, A. Raina, A phase-field model for chemo-mechanical induced fracture in lithium-ion battery electrode particles, Int. J. Numer. Methods Eng. 106 (9) (2016) 683–711.

[74] S. Abada, M. Petit, A. Lecocq, G. Marlair, V. Sauvant-Moynot, F. Huet, Combined experimental and modeling approaches of the thermal runaway of fresh and aged lithium-ion batteries, J. Power Sources 399 (2018) 264–273.

[75] G. Liu, W. Lu, A model of concurrent lithium dendrite growth, sei growth, sei penetration and regrowth, J. Electrochem. Soc. 164 (9) (2017) A1826.

[76] L. Liang, Y. Qi, F. Xue, S. Bhattacharya, S.J. Harris, L.-Q. Chen, Nonlinear phase-field model for electrode-electrolyte interface evolution, Phys. Rev. E 86 (5) (2012), 051609.

[77] K. Wang, Y. Xiao, P. Pei, X. Liu, Y. Wang, A phase-field model of dendrite growth of electrodeposited zinc, J. Electrochem. Soc. 166 (10) (2019) D389.

[78] Y. Gao, J. Jiang, C. Zhang, W. Zhang, Z. Ma, Y. Jiang, Lithium-ion battery aging mechanisms and life model under different charging stresses, J. Power Sources 356 (2017) 103–114.

[79] L. Su, J. Zhang, C. Wang, Y. Zhang, Z. Li, Y. Song, T. Jin, Z. Ma, Identifying main factors of capacity fading in lithium ion cells using orthogonal design of experiments, Appl. Energy 163 (2016) 201–210.

[80] S.S. Zhang, The effect of the charging protocol on the cycle life of a Li-ion battery, J. Power Sources 161 (2) (2006) 1385–1391.

[81] S.S. Choi, H.S. Lim, Factors that affect cycle-life and possible degradation mechanisms of a Li-ion cell based on licoo2, J. Power Sources 111 (1) (2002) 130–136.
[82] S. Saxena, C. Hendricks, M. Pecht, Cycle life testing and modeling of graphite/LiCoO2 cells under different state of charge ranges, J. Power Sources 327 (2016) 394–400.
[83] R.P. Ramasamy, R.E. White, B.N. Popov, Calendar life performance of pouch lithium-ion cells, J. Power Sources 141 (2) (2005) 298–306.
[84] F. Leng, C.M. Tan, M. Pecht, Effect of temperature on the aging rate of Li ion battery operating above room temperature, Sci. Rep. 5 (2015) 12967.
[85] C. Akkaldevi, S.D. Chitta, J. Jaidi, S. Panchal, M. Fowler, R. Fraser, Coupled electrochemical-thermal simulations and validation of minichannel cold-plate water-cooled prismatic 20 ah lifepo4 battery, Electrochem 2 (4) (2021) 643–663.
[86] V. Choudhari, A. Dhoble, S. Panchal, M. Fowler, R. Fraser, Numerical investigation on thermal behaviour of 5 5 cell configured battery pack using phase change material and fin structure layout, J. Energy Storage 43 (2021), 103234.
[87] S.D. Chitta, C. Akkaldevi, J. Jaidi, S. Panchal, M. Fowler, R. Fraser, Comparison of lumped and 1d electrochemical models for prismatic 20ah lifepo4 battery sandwiched between minichannel cold-plates, Appl. Therm. Eng. 199 (2021), 117586.
[88] T. Waldmann, M. Wilka, M. Kasper, M. Fleischhammer, M. Wohlfahrt-Mehrens, Temperature dependent ageing mechanisms in lithium-ion batteries–a post-mortem study, J. Power Sources 262 (2014) 129–135.
[89] S. Zhang, K. Xu, T. Jow, Electrochemical impedance study on the low temperature of Li-ion batteries, Electrochim. Acta 49 (7) (2004) 1057–1061.
[90] M. Ouyang, Z. Chu, L. Lu, J. Li, X. Han, X. Feng, G. Liu, Low temperature aging mechanism identification and lithium deposition in a large format lithium iron phosphate battery for different charge profiles, J. Power Sources 286 (2015) 309–320.
[91] S. Watanabe, M. Kinoshita, T. Hosokawa, K. Morigaki, K. Nakura, Capacity fading of LiAlyNi1- x- yCoxO2 cathode for lithium-ion batteries during accelerated calendar and cycle life tests (effect of depth of discharge in charge–discharge cycling on the suppression of the micro-crack generation of LiAlyNi1- x- yCoxO2 particle), J. Power Sources 260 (2014) 50–56.
[92] N. Omar, M.A. Monem, Y. Firouz, J. Salminen, J. Smekens, O. Hegazy, H. Gaulous, G. Mulder, P. Van den Bossche, T. Coosemans, et al., Lithium iron phosphate based battery–assessment of the aging parameters and development of cycle life model, Appl. Energy 113 (2014) 1575–1585.
[93] J. de Hoog, J.-M. Timmermans, D. Ioan-Stroe, M. Swierczynski, J. Jaguemont, S. Goutam, N. Omar, J. Van Mierlo, P. Van Den Bossche, Combined cycling and calendar capacity fade modeling of a nickel-manganese-cobalt oxide cell with real-life profile validation, Appl. Energy 200 (2017) 47–61.
[94] J.R. Belt, C.D. Ho, C.G. Motloch, T.J. Miller, T.Q. Duong, A capacity and power fade study of Li-ion cells during life cycle testing, J. Power Sources 123 (2) (2003) 241–246.
[95] M. Ouyang, D. Ren, L. Lu, J. Li, X. Feng, X. Han, G. Liu, Overcharge-induced capacity fading analysis for large format lithium-ion batteries with liyni1/3co1/3mn1/3o2+ liymn2o4 composite cathode, J. Power Sources 279 (2015) 626–635.
[96] J. Schmalstieg, S. Käbitz, M. Ecker, D.U. Sauer, A holistic aging model for Li (NiMnCo)O2 based 18650 lithium-ion batteries, J. Power Sources 257 (2014) 325–334.
[97] R. Guo, L. Lu, M. Ouyang, X. Feng, Mechanism of the entire overdischarge process and overdischarge-induced internal short circuit in lithium-ion batteries, Sci. Rep. 6 (1) (2016) 1–9.
[98] M. Broussely, P. Biensan, F. Bonhomme, P. Blanchard, S. Herreyre, K. Nechev, R. Staniewicz, Main aging mechanisms in Li ion batteries, J. Power Sources 146 (1–2) (2005) 90–96.
[99] J. Belt, V. Utgikar, I. Bloom, Calendar and PHEV cycle life aging of high-energy, lithium-ion cells containing blended spinel and layered-oxide cathodes, J. Power Sources 196 (23) (2011) 10213–10221.
[100] H.J. Ploehn, P. Ramadass, R.E. White, Solvent diffusion model for aging of lithium-ion battery cells, J. Electrochem. Soc. 151 (3) (2004) A456–A462.
[101] R. Hausbrand, G. Cherkashinin, H. Ehrenberg, M. Gröting, K. Albe, C. Hess, W. Jaegermann, Fundamental degradation mechanisms of layered oxide Li-ion battery cathode materials: methodology, insights and novel approaches, Mater. Sci. Eng. B 192 (2015) 3–25.
[102] S.F. Schuster, T. Bach, E. Fleder, J. Müller, M. Brand, G. Sextl, A. Jossen, Nonlinear aging characteristics of lithium-ion cells under different operational conditions, J. Energy Storage 1 (2015) 44–53.
[103] J. Cannarella, C.B. Arnold, Stress evolution and capacity fade in constrained lithium-ion pouch cells, J. Power Sources 245 (2014) 745–751.
[104] Z. Li, J. Huang, B.Y. Liaw, V. Metzler, J. Zhang, A review of lithium deposition in lithium-ion and lithium metal secondary batteries, J. Power Sources 254 (2014) 168–182.
[105] J. Christensen, J. Newman, Cyclable lithium and capacity loss in Li-ion cells, J. Electrochem. Soc. 152 (4) (2005), A818.
[106] A. Farmann, W. Waag, A. Marongiu, D.U. Sauer, Critical review of on-board capacity estimation techniques for lithium-ion batteries in electric and hybrid electric vehicles, J. Power Sources 281 (2015) 114–130.
[107] C. Weng, Y. Cui, J. Sun, H. Peng, On-board state of health monitoring of lithium-ion batteries using incremental capacity analysis with support vector regression, J. Power Sources 235 (2013) 36–44.
[108] M. Safari, C. Delacourt, Aging of a commercial graphite/LiFePO4 cell, J. Electrochem. Soc. 158 (10) (2011) A1123.
[109] X. Li, Z. Wang, L. Zhang, C. Zou, D.D. Dorrell, State-of-health estimation for Li-ion batteries by combing the incremental capacity analysis method with grey relational analysis, J. Power Sources 410 (2019) 106–114.
[110] J. Tian, R. Xiong, Q. Yu, Fractional-order model-based incremental capacity analysis for degradation state recognition of lithium-ion batteries, IEEE Trans. Ind. Electron. 66 (2) (2018) 1576–1584.
[111] M. Lewerenz, D.U. Sauer, Evaluation of cyclic aging tests of prismatic automotive linimncoo2-graphite cells considering influence of homogeneity and anode overhang, J. Energy Storage 18 (2018) 421–434.
[112] S.K. Rechkemmer, X. Zang, W. Zhang, O. Sawodny, Calendar and cycle aging study of a commercial limn2o4 cell under consideration of influences by cell progress, J. Energy Storage 30 (2020), 101547.
[113] Y. Gao, J. Jiang, C. Zhang, W. Zhang, Y. Jiang, Aging mechanisms under different state-of-charge ranges and the multi-indicators system of state-of-health for lithium-ion battery with Li (nimnco) o2 cathode, J. Power Sources 400 (2018) 641–651.
[114] M. Dubarry, C. Truchot, B.Y. Liaw, Synthesize battery degradation modes via a diagnostic and prognostic model, J. Power Sources 219 (2012) 204–216.
[115] D. Anseán, V.M. García, M. González, C. Blanco-Viejo, J.C. Viera, Y.F. Pulido, L. Sánchez, Lithium-ion battery degradation indicators via incremental capacity analysis, IEEE Trans. Ind. Appl. 55 (3) (2019) 2992–3002.
[116] X. Han, M. Ouyang, L. Lu, J. Li, Cycle life of commercial lithium-ion batteries with lithium titanium oxide anodes in electric vehicles, Energies 7 (8) (2014) 4895–4909.
[117] I. Bloom, L.K. Walker, J.K. Basco, D.P. Abraham, J.P. Christophersen, C.D. Ho, Differential voltage analyses of high-power lithium-ion cells. 4. Cells containing nmc, J. Power Sources 195 (3) (2010) 877–882.
[118] Y. Li, M. Abdel-Monem, R. Gopalakrishnan, M. Berecibar, E. Nanini-Maury, N. Omar, P. van den Bossche, J. Van Mierlo, A quick on-line state of health estimation method for Li-ion battery with incremental capacity curves processed by gaussian filter, J. Power Sources 373 (2018) 40–53.
[119] T. Shibagaki, Y. Merla, G.J. Offer, Tracking degradation in lithium iron phosphate batteries using differential thermal voltammetry, J. Power Sources 374 (2018) 188–195.
[120] M. Berecibar, M. Garmendia, I. Gandiaga, J. Crego, I. Villarreal, State of health estimation algorithm of lifepo4 battery packs based on differential voltage curves for battery management system application, Energy 103 (2016) 784–796.
[121] J. Zhu, M.S.D. Darma, M. Knapp, D.R. Sørensen, M. Heere, Q. Fang, X. Wang, H. Dai, L. Mereacre, A. Senyshyn, et al., Investigation of lithium-ion battery degradation mechanisms by combining differential voltage analysis and alternating current impedance, J. Power Sources 448 (2020), 227575.
[122] S. Zhang, X. Guo, X. Dou, X. Zhang, A rapid online calculation method for state of health of lithium-ion battery based on coulomb counting method and differential voltage analysis, J. Power Sources 479 (2020), 228740.
[123] Q. Zhang, X. Li, Z. Du, Q. Liao, Aging performance characterization and state-of-health assessment of retired lithium-ion battery modules, J. Energy Storage 40 (2021), 102743.
[124] C. Weng, J. Sun, H. Peng, A unified open-circuit-voltage model of lithium-ion batteries for state-of-charge estimation and state-of-health monitoring, J. Power Sources 258 (2014) 228–237.
[125] L. Wang, X. Zhao, L. Liu, C. Pan, State of health estimation of battery modules via differential voltage analysis with local data symmetry method, Electrochim. Acta 256 (2017) 81–89.
[126] L. Wang, C. Pan, L. Liu, Y. Cheng, X. Zhao, On-board state of health estimation of LiFePO4 battery pack through differential voltage analysis, Appl. Energy 168 (2016) 465–472.
[127] X. Hu, W. Liu, X. Lin, Y. Xie, A comparative study of control-oriented thermal models for cylindrical Li-ion batteries, IEEE Trans. Transp. Electrif. 5 (4) (2019) 1237–1253.
[128] G.L. Plett, Extended kalman filtering for battery management systems of LiPB-based HEV battery packs: part 3. State and parameter estimation, J. Power Sources 134 (2) (2004) 277–292.
[129] J. Li, N. Lotfi, R.G. Landers, J. Park, A single particle model for lithium-ion batteries with electrolyte and stress-enhanced diffusion physics, J. Electrochem. Soc. 164 (4) (2017) A874.
[130] J. Li, R.G. Landers, J. Park, A comprehensive single-particle-degradation model for battery state-of-health prediction, J. Power Sources 456 (2020), 227950.
[131] Y. Gao, X. Zhang, J. Yang, B. Guo, Estimation of state-of-charge and state-of-health for lithium-ion degraded battery considering side reactions, J. Electrochem. Soc. 165 (16) (2018), A4018.
[132] Y. Bi, Y. Yin, S.-Y. Choe, Online state of health and aging parameter estimation using a physics-based life model with a particle filter, J. Power Sources 476 (2020), 228655.
[133] T.R. Tanim, C.D. Rahn, Aging formula for lithium ion batteries with solid electrolyte interphase layer growth, J. Power Sources 294 (2015) 239–247.
[134] T. Mesbahi, N. Rizoug, P. Bartholomeüs, R. Sadoun, F. Khenfri, P. Le Moigne, Dynamic model of li-ion batteries incorporating electrothermal and ageing aspects for electric vehicle applications, IEEE Trans. Ind. Electron. 65 (2) (2018) 1298–1305.
[135] M. Ecker, J.B. Gerschler, J. Vogel, S. Käbitz, F. Hust, P. Dechent, D.U. Sauer, Development of a lifetime prediction model for lithium-ion batteries based on extended accelerated aging test data, J. Power Sources 215 (2012) 248–257.
[136] M.-K. Tran, M. Mathew, S. Janhunen, S. Panchal, K. Raahemifar, R. Fraser, M. Fowler, A comprehensive equivalent circuit model for lithium-ion batteries, incorporating the effects of state of health, state of charge, and temperature on model parameters, J. Energy Storage 43 (2021), 103252.

[137] H.E. Perez, X. Hu, S. Dey, S.J. Moura, Optimal charging of li-ion batteries with coupled electro-thermal-aging dynamics, IEEE Trans. Veh. Technol. 66 (9) (2017) 7761–7770.
[138] X. Hu, Y. Zheng, X. Lin, Y. Xie, Optimal multistage charging of nca/graphite lithium-ion batteries based on electrothermal-aging dynamics, IEEE Trans. Transp. Electrif. 6 (2) (2020) 427–438.
[139] A. Cordoba-Arenas, S. Onori, Y. Guezennec, G. Rizzoni, Capacity and power fade cycle-life model for plug-in hybrid electric vehicle lithium-ion battery cells containing blended spinel and layered-oxide positive electrodes, J. Power Sources 278 (2015) 473–483.
[140] J. Wang, P. Liu, J. Hicks-Garner, E. Sherman, S. Soukiazian, M. Verbrugge, H. Tataria, J. Musser, P. Finamore, Cycle-life model for graphite-LiFePO4 cells, J. Power Sources 196 (8) (2011) 3942–3948.
[141] M. Swierczynski, D.-I. Stroe, A.-I. Stan, R. Teodorescu, S.K. Kær, Lifetime estimation of the nanophosphate battery chemistry used in fully electric vehicles, IEEE Trans. Ind. Appl. 51 (4) (2015) 3453–3461.
[142] D.-I. Stroe, M. Świerczyński, A.-I. Stan, R. Teodorescu, S.J. Andreasen, Accelerated lifetime testing methodology for lifetime estimation of lithium-ion batteries used in augmented wind power plants, IEEE Trans. Ind. Appl. 50 (6) (2014) 4006–4017.
[143] D.-I. Stroe, M. Swierczynski, S.K. Kær, R. Teodorescu, Degradation behavior of lithium-ion batteries during calendar ageing—the case of the internal resistance increase, IEEE Trans. Ind. Appl. 54 (1) (2017) 517–525.
[144] F. Todeschini, S. Onori, G. Rizzoni, An experimentally validated capacity degradation model for Li-ion batteries in PHEVs applications, IFAC Proceedings Volumes 45 (20) (2012) 456–461.
[145] S. Grolleau, A. Delaille, H. Gualous, P. Gyan, R. Revel, J. Bernard, E. Redondo-Iglesias, J. Peter, S. Network, Calendar aging of commercial graphite/lifepo4 cell–predicting capacity fade under time dependent storage conditions, J. Power Sources 255 (2014) 450–458.
[146] G. Zubi, R. Dufo-López, M. Carvalho, G. Pasaoglu, The lithium-ion battery: state of the art and future perspectives, Renew. Sust. Energ. Rev. 89 (2018) 292–308.
[147] M. Jafari, K. Khan, L. Gauchia, Deterministic models of Li-ion battery aging: it is a matter of scale, J. Energy Storage 20 (2018) 67–77.
[148] A. Ahmadian, M. Sedghi, A. Elkamel, M. Fowler, M.A. Golkar, Plug-in electric vehicle batteries degradation modeling for smart grid studies: review, assessment and conceptual framework, Renew. Sust. Energ. Rev. 81 (2018) 2609–2624.
[149] J. Tian, R. Xu, Y. Wang, Z. Chen, Capacity attenuation mechanism modeling and health assessment of lithium-ion batteries, Energy 221 (2021), 119682.
[150] T. Goh, M. Park, M. Seo, J.G. Kim, S.W. Kim, Capacity estimation algorithm with a second-order differential voltage curve for Li-ion batteries with nmc cathodes, Energy 135 (2017) 257–268.
[151] H. Pan, Z. Lü, H. Wang, H. Wei, L. Chen, Novel battery state-of-health online estimation method using multiple health indicators and an extreme learning machine, Energy 160 (2018) 466–477.
[152] B. Jia, Y. Guan, L. Wu, A state of health estimation framework for lithium-ion batteries using transfer components analysis, Energies 12 (13) (2019) 2524.
[153] V. Klass, M. Behm, G. Lindbergh, A support vector machine-based state-of-health estimation method for lithium-ion batteries under electric vehicle operation, J. Power Sources 270 (2014) 262–272.
[154] A. Nuhic, T. Terzimehic, T. Soczka-Guth, M. Buchholz, K. Dietmayer, Health diagnosis and remaining useful life prognostics of lithium-ion batteries using data-driven methods, J. Power Sources 239 (2013) 680–688.
[155] D. Andre, C. Appel, T. Soczka-Guth, D.U. Sauer, Advanced mathematical methods of soc and soh estimation for lithium-ion batteries, J. Power Sources 224 (2013) 20–27.
[156] A. Zenati, P. Desprez, H. Razik, Estimation of the SOC and the SOH of li-ion batteries, by combining impedance measurements with the fuzzy logic inference, in: IECON 2010-36th Annual Conference on IEEE Industrial Electronics Society, IEEE, 2010, pp. 1773–1778.
[157] K. Yang, Z. Chen, Z. He, Y. Wang, Z. Zhou, Online estimation of state of health for the airborne li-ion battery using adaptive dekf-based fuzzy inference system, Soft. Comput. (2020) 1–10.
[158] D. Liu, J. Pang, J. Zhou, Y. Peng, M. Pecht, Prognostics for state of health estimation of lithium-ion batteries based on combination gaussian process functional regression, Microelectron. Reliab. 53 (6) (2013) 832–839.
[159] X. Qin, Q. Zhao, H. Zhao, W. Feng, X. Guan, Prognostics of remaining useful life for lithium-ion batteries based on a feature vector selection and relevance vector machine approach, in: 2017 IEEE International Conference on Prognostics and Health Management (ICPHM), IEEE, 2017, pp. 1–6.
[160] Y. Che, Z. Deng, X. Lin, L. Hu, X. Hu, Predictive battery health management with transfer learning and online model correction, IEEE Trans. Veh. Technol. 70 (2) (2021) 1269–1277.
[161] Y. Fan, F. Xiao, C. Li, G. Yang, X. Tang, A novel deep learning framework for state of health estimation of lithium-ion battery, J. Energy Storage 32 (2020), 101741.
[162] S. Shen, M. Sadoughi, X. Chen, M. Hong, C. Hu, A deep learning method for online capacity estimation of lithium-ion batteries, J. Energy Storage 25 (2019), 100817.
[163] K. Kaur, A. Garg, X. Cui, S. Singh, B.K. Panigrahi, Deep learning networks for capacity estimation for monitoring soh of Li-ion batteries for electric vehicles, Int. J. Energy Res. 45 (2) (2021) 3113–3128.
[164] W. Pan, X. Luo, M. Zhu, J. Ye, L. Gong, H. Qu, A health indicator extraction and optimization for capacity estimation of Li-ion battery using incremental capacity curves, J. Energy Storage 42 (2021), 103072.
[165] J.-Z. Kong, F. Yang, X. Zhang, E. Pan, Z. Peng, D. Wang, Voltage-temperature health feature extraction to improve prognostics and health management of lithium-ion batteries, Energy 223 (2021), 120114.
[166] Z. Deng, X. Hu, X. Lin, L. Xu, Y. Che, L. Hu, General discharge voltage information enabled health evaluation for lithium-ion batteries, IEEE/ASME Transactions on Mechatronics.
[167] P. Guo, Z. Cheng, L. Yang, A data-driven remaining capacity estimation approach for lithium-ion batteries based on charging health feature extraction, J. Power Sources 412 (2019) 442–450.
[168] L. Liao, F. Köttig, Review of hybrid prognostics approaches for remaining useful life prediction of engineered systems, and an application to battery life prediction, IEEE Trans. Reliab. 63 (1) (2014) 191–207.
[169] J. Wei, G. Dong, Z. Chen, Remaining useful life prediction and state of health diagnosis for lithium-ion batteries using particle filter and support vector regression, IEEE Trans. Ind. Electron. 65 (7) (2017) 5634–5643.
[170] X. Zheng, H. Fang, An integrated unscented kalman filter and relevance vector regression approach for lithium-ion battery remaining useful life and short-term capacity prediction, Reliab. Eng. Syst. Saf. 144 (2015) 74–82.
[171] Z. Ma, R. Yang, Z. Wang, A novel data-model fusion state-of-health estimation approach for lithium-ion batteries, Appl. Energy 237 (2019) 836–847.
[172] D. Liu, X. Yin, Y. Song, W. Liu, Y. Peng, An on-line state of health estimation of lithium-ion battery using unscented particle filter, IEEE Access 6 (2018) 40990–41001.
[173] S. Li, H. He, C. Su, P. Zhao, Data driven battery modeling and management method with aging phenomenon considered, Appl. Energy 275 (2020), 115340.
[174] C. Hu, B.D. Youn, P. Wang, J.T. Yoon, Ensemble of data-driven prognostic algorithms for robust prediction of remaining useful life, Reliab. Eng. Syst. Saf. 103 (2012) 120–135.
[175] Z. Chen, Q. Xue, R. Xiao, Y. Liu, J. Shen, State of health estimation for lithium-ion batteries based on fusion of autoregressive moving average model and elman neural network, IEEE Access 7 (2019) 102662–102678.
[176] X. Feng, J. Li, M. Ouyang, L. Lu, J. Li, X. He, Using probability density function to evaluate the state of health of lithium-ion batteries, J. Power Sources 232 (2013) 209–218.
[177] B. Gou, Y. Xu, X. Feng, State-of-health estimation and remaining-useful-life prediction for lithium-ion battery using a hybrid data-driven method, IEEE Trans. Veh. Technol. 69 (10) (2020) 10854–10867.
[178] Y. Song, D. Liu, H. Liao, Y. Peng, A hybrid statistical data-driven method for on-line joint state estimation of lithium-ion batteries, Appl. Energy 261 (2020), 114408.
[179] M. Dubarry, D. Beck, Big data training data for artificial intelligence-based Li-ion diagnosis and prognosis, J. Power Sources 479 (2020), 228806.
[180] K.S. Mayilvahanan, K.J. Takeuchi, E.S. Takeuchi, A.C. Marschilok, A.C. West, Supervised learning of synthetic big data for Li-ion battery degradation diagnosis, Batteries Supercaps 5 (1) (2022), e202100166.
[181] M. Kabir, D.E. Demirocak, Degradation mechanisms in Li-ion batteries: a state-of-the-art review, Int. J. Energy Res. 41 (14) (2017) 1963–1986.
[182] B. Stiaszny, J.C. Ziegler, E.E. Krauss, J.P. Schmidt, E. Ivers-Tiffée, Electrochemical characterization and post-mortem analysis of aged LiMn2O4–Li (Ni0. 5Mn0. 3Co0. 2) O2/graphite lithium ion batteries. Part i: cycle aging, J. Power Sources 251 (2014) 439–450.
[183] S.S. Zhang, K. Xu, T. Jow, Study of the charging process of a LiCoO2-based Li-ion battery, J. Power Sources 160 (2) (2006) 1349–1354.
[184] A.M. Colclasure, K.A. Smith, R.J. Kee, Modeling detailed chemistry and transport for solid-electrolyte-interface (SEI) films in Li–ion batteries, Electrochim. Acta 58 (2011) 33–43.
[185] J.M. Reniers, G. Mulder, D.A. Howey, Review and performance comparison of mechanical-chemical degradation models for lithium-ion batteries, J. Electrochem. Soc. 166 (14) (2019) A3189.
[186] U. Janakiraman, T.R. Garrick, M.E. Fortier, Lithium plating detection methods in Li-ion batteries, J. Electrochem. Soc. 167 (16) (2020), 160552.
[187] X. Zhang, J. Lu, S. Yuan, J. Yang, X. Zhou, A novel method for identification of lithium-ion battery equivalent circuit model parameters considering electrochemical properties, J. Power Sources 345 (2017) 21–29.
[188] G. Vennam, A. Sahoo, Simultaneous state and parameter estimation of lithium-ion battery: An observer based approach, in: 2019 American Control Conference (ACC), IEEE, 2019, pp. 4485–4490.
[189] A. Sahoo, V. Narayanan, Differential-game for resource aware approximate optimal control of large-scale nonlinear systems with multiple players, Neural Netw. 124 (2020) 95–108.
[190] W. Yan, B. Zhang, G. Zhao, S. Tang, G. Niu, X. Wang, A battery management system with a lebesgue-sampling-based extended kalman filter, IEEE Trans. Ind. Electron. 66 (4) (2018) 3227–3236.
[191] L. Zheng, J. Zhu, D.D.-C. Lu, G. Wang, T. He, Incremental capacity analysis and differential voltage analysis based state of charge and capacity estimation for lithium-ion batteries, Energy 150 (2018) 759–769.